

# A Revolution in Electrodes: Recent Progress in Rechargeable Lithium–Sulfur Batteries

Xin Fang and Huisheng Peng\*



## From the Contents

1. Introduction .....	1489
2. Sulfur Cathodes .....	1491
3. Anodes .....	1503
4. Flexible Electrodes .....	1506
5. Challenges and Perspectives .....	1506

**A**s a promising candidate for future batteries, the lithium–sulfur battery is gaining increasing interest due to its high capacity and energy density. However, over the years, lithium–sulfur batteries have been plagued by fading capacities and the low Coulombic efficiency derived from its unique electrochemical behavior, which involves solid–liquid transition reactions. Moreover, lithium–sulfur batteries employ metallic lithium as the anode, which engenders safety vulnerability of the battery. The electrodes play a pivotal role in the performance of lithium–sulfur batteries. A leap forward in progress of lithium–sulfur batteries is always accompanied by a revolution in the electrode technology. In this review, recent progress in rechargeable lithium–sulfur batteries is summarized in accordance with the evolution of the electrodes, including the diversified cathode design and burgeoning metallic-lithium-free anodes. Although the way toward application has still many challenges associated, recent progress in lithium–sulfur battery technology still paints an encouraging picture of a revolution in rechargeable batteries.

## 1. Introduction

It is probably not good news that lithium-ion batteries are nearing their ceiling performance. Many researchers believe that technical optimization can at most squeeze 30% more energy from lithium-ion batteries, which means that lithium-ion batteries can never reach the goal of an on-board battery enabling electric vehicles to drive more than 800 km before needing to be recharged. Moreover, today's portable devices, mobile phones, laptops, and digital cameras, are powered by lithium-ion batteries. It is fair for consumers to charge a handset once a day. In the case of state-of-the-art wearable devices, however, the traditional battery seems unable to afford a satisfying longevity.<sup>[1–5]</sup> Admittedly, battery longevity is a formidable problem that plagues all portable devices. A revolution in batteries is required, to leap beyond the capabilities of lithium-ion batteries, which has triggered the renaissance of a veteran energy-storage system: the lithium–sulfur battery.

The concept of the lithium–sulfur battery emerged in the 1960s.<sup>[6]</sup> As a promising successor to lithium-ion batteries, the lithium–sulfur battery has experienced an upsurge in interest and has also endured a period of recession in development. Just as its name implies, the lithium–sulfur battery stores and delivers energy through the reversible electrochemical reaction between lithium and sulfur. The capability of storing energy is indexed by the energy density, which represents the superiority of the lithium–sulfur battery. In theory, the lithium–sulfur battery (2600 W h kg<sup>-1</sup>) can hold as much as five times the energy density of commercial batteries. Its theoretical capacity, 1675 mA h g<sup>-1</sup>, based on the active materials, is an order of magnitude higher than that of conventional batteries, and is derived from the conversion whereby one sulfur atom is incorporated with two lithium atoms yielding the lithiated product Li<sub>2</sub>S. As traditional batteries lose their attractiveness in electrical vehicles and portable devices, the lithium–sulfur battery is back in vogue.

### 1.1. Working Mechanism

The general reaction of the lithium–sulfur battery is given:



When the battery is discharged, lithium ions migrate toward the cathode and react with sulfur to produce lithiated polysulfide compounds (Li<sub>2</sub>S<sub>x</sub>). The discharge process involves two stages of reaction, which correspond to the two plateaus in voltage profile, as well as the two cathodic peaks in the cyclic voltammogram. As displayed in **Figure 1a**, the higher plateau is situated at 2.2–2.3 V, which relates to the production of high-order polysulfides:



High-order polysulfides (Li<sub>2</sub>S<sub>x</sub>, x ≥ 4) are soluble in the electrolyte, so the first plateau entails a solid–liquid transition.

The dissolution of sulfur is critical to the performance of the battery, which refreshes the surface and exposes the internal sulfur for reduction. On the other hand, soluble polysulfides are prone to diffuse out of the cathode, and this leads to the irreversible loss of active materials. As a result, the sulfur electrode is gradually fragmented and the battery degraded as it is recharged. The lower plateau at 1.9–2.1 V corresponds to the deposition of low-order lithium–sulfur compounds:



As the sulfur chain shortens, the solubility of the compound decreases, and the viscosity of the electrolyte increases until the deposition of insoluble Li<sub>2</sub>S. The liquid–solid transition of the lithium–sulfur compounds contributes the dominant capacity of the battery, as manifested by the prolonged plateau at the lower stage. Since the diffusion of soluble compounds engenders the loss of active materials, it is understandable that the capacity delivered by the second plateau suffers a major decay over cycling.

The liquid–solid transition of lithium–sulfur compounds leads to the unique electrochemical behavior of lithium–sulfur batteries. The electrode morphology is dramatically changed in the repeated dissolution and deposition process, which is compounded by another problem that the density difference of sulfur (2.07 g cm<sup>-3</sup>) and Li<sub>2</sub>S (1.66 g cm<sup>-3</sup>) brings about a volume change. The nucleation of Li<sub>2</sub>S causes the redistribution of active materials, some of which divorce from the conducting matrix, causing an irreversible loss. In this case, the initial status of sulfur in the cathode is of limited importance since the redistribution of Li<sub>2</sub>S is inevitable.<sup>[7–9]</sup> Qiu and co-workers investigated the discharge process using electrochemical impedance spectroscopy and found that Li<sub>2</sub>S appeared immediately at the beginning of the lower plateau,<sup>[10]</sup> which was backed up by in situ X-ray diffraction characterization.<sup>[11]</sup> Based on the solid–liquid transition of lithium–sulfur compounds during discharge, Manthiram and co-workers proposed an innovative strategy to cope with the fading of capacity during repeated drain and recharge processes (Figure 1b).<sup>[12]</sup> Since the soluble polysulfides that are produced at the higher plateau are to blame for the irreversible loss of capacity, they terminated the recharge process at the start of the lower plateau. Afterward, the electrochemical reaction was manipulated within the region of the lower plateau, where the deposition of Li<sub>2</sub>S occurred, and

X. Fang, Prof. H. Peng  
State Key Laboratory of Molecular  
Engineering of Polymers  
Department of Macromolecular Science  
and Laboratory of Advanced Materials  
Fudan University  
Shanghai 200438, China  
E-mail: penghs@fudan.edu.cn



DOI: 10.1002/smll.201402354

which dominantly delivered the capacity ( $1256 \text{ mA h g}^{-1}$  in theory). As previously mentioned,  $\text{Li}_2\text{S}_4$  is less soluble than its long-chain analogues, so when the reaction was ring-fenced between  $\text{Li}_2\text{S}_4$  and  $\text{Li}_2\text{S}$  by a recharge programme, the lithium–sulfur compounds can hardly seep into the electrolyte. This strategy significantly extended the cycle life of the battery, whose capacity decayed by 0.53% over 500 cycles, suggesting the active materials were well retained in the cathode.

### 1.2. Problems

The investigation of lithium–sulfur batteries started several decades ago. However, unlike their analogues, where lithium ions shuttle between graphite and metal oxide electrodes, the academic interest of the lithium–sulfur battery has not yet been translated into commercial success. The inferior cyclic stability is the major problem that retards its step toward applications. In the long period since its emergence, researchers have wrestled with the tricky issues that make the battery suffocate within dozens of cycles.<sup>[13]</sup>

- (1) Isolated sulfur: elemental sulfur and its lithiated compounds ( $\text{Li}_2\text{S}$ ) are intrinsically non-conducting, which makes it hard for them to accept electrons from the current collector. Therefore, the theoretical capacity is rarely achieved due to the limited utilization of sulfur, even though the conducting agent is added. Moreover, electrochemical kinetics are affected by the large resistance of the electrode, leading to large polarization and inferior rate capability. In this respect, the conducting matrix plays a pivotal role to ensure a high capacity and rate performance.
- (2) Soluble polysulfides: as discussed before, long-chain lithium–sulfur compounds ( $\text{Li}_2\text{S}_x$ ,  $x = 4\text{--}8$ ) are soluble in the electrolyte. The dissolution of polysulfide renews the sulfur surface and facilitates reduction. Meanwhile, they are inclined to diffuse out from the cathode, driven by the concentration gradient, which leads to degradation of capacity. As the battery cycles, the viscosity is increased and the electrolyte is saturated; thus, the migration of polysulfides will then be alleviated. Accordingly, increasing the concentration of lithium salt in the electrolyte can suppress the dissolution and diffusion of polysulfides, which is a simple and effective strategy of enhancing the stability of the lithium–sulfur battery.<sup>[14,15]</sup> On the other hand, controlling the ratio between the electrolyte and sulfur can also improve its cyclic performance. The limited amount of electrolyte counteracts the dissolution equilibrium between the cathode and electrolyte, suppressing the diffusion of polysulfides and alleviating the capacity decay.<sup>[16,17]</sup>
- (3) Shuttle effect: the shuttle effect is the primary deterioration mechanism for lithium–sulfur batteries. It is derived from the dissolution and diffusion of polysulfides that are prone to react with the lithium anode and thus be reduced to lower-order polysulfides. The lower-order polysulfides



**Xin Fang** received his B.S. in Polymer Material and Engineering from Sichuan University in 2012. He is currently a graduate student majoring at Macromolecular Chemistry and Physics at Fudan University. His work focuses on the synthesis of carbon nanomaterials and their applications in energy conversion and storage.



**Huisheng Peng** is currently a professor at the Department of Macromolecular Science and Laboratory of Advanced Materials at Fudan University. He received his B.E. in Polymer Materials at Donghua University in China in 1999, M.S. in Macromolecular Chemistry and Physics at Fudan University in China in 2003 and Ph.D. in Chemical Engineering at Tulane University in USA in 2006. He then worked at Los Alamos National Laboratory before joining Fudan University in 2008. He focuses on the development of miniature wire-shaped solar cells, lithium-ion batteries, and supercapacitors.

then migrate back to the cathode and are recharged to higher-order polysulfides. The shuttle effect describes the phenomenon that part of the dissolved polysulfides are constantly shuttled and converted between the two electrodes, which as a consequence, makes the charging process hesitate in the lower plateau region and become significantly prolonged, rendering a low Coulombic efficiency. The shuttle effect is a major problem that degrades the battery. Recently, however, it has been found that additives in the electrolyte,  $\text{LiNO}_3$  for example, can create a passivation film on the lithium anode, which is conducive to suppressing surface reactions and inhibiting the shuttle effect.<sup>[18–20]</sup>

- (4) Morphology reconstruction: since the electrochemical process in lithium–sulfur battery entails a solid–liquid–solid transition, repeated nucleation and dissolution will exert a significant impact on the morphology of the electrode. The active materials will redistribute in the cathode and those isolated from the conducting matrix hence become inactive. The redistribution is complicated by the volume expansion, as we have discussed, which leads to the reconstruction of the cathode morphology, thoroughly different from its initial status.

Indeed, lithium–sulfur batteries are plagued by a series of problems that cloud their future. After a couple of years of stagnation, researchers hope to resuscitate the lithium–sulfur battery motivated by the ever-growing needs for densified energy-storage systems beyond the scope of lithium-ion batteries. Over the last few years, achievements in squeezing the capacity and enhancing the cyclic stability have become

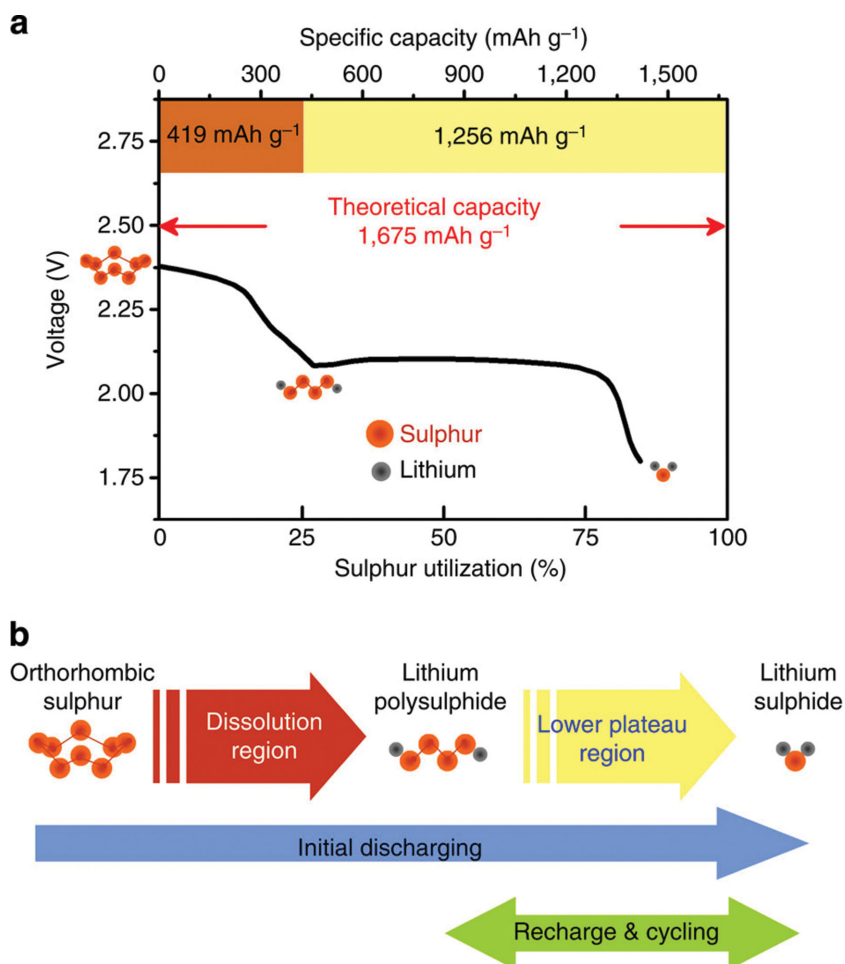


**Figure 1.** a) Typical discharge voltage profile of a lithium–sulfur battery. b) Recharge strategy for prolonging the cycle life of the lithium–sulfur battery. Reproduced with permission.<sup>[12]</sup> Copyright 2013, Nature Publishing Group.

routine in this fiercely-progressed field, which paints an encouraging picture for the application of lithium–sulfur batteries pertaining to electrical vehicles and portable devices. The revolution in electrodes, undoubtedly raises interest in the investigation of lithium–sulfur batteries.

## 2. Sulfur Cathodes

In lithium–sulfur batteries, the electrochemical reactions primarily take place in the sulfur cathode. The sulfur cannot serve as cathode individually because of its isolation nature and soluble compounds, which necessitates a second component as a conducting matrix and sulfur host. Generally, an eligible sulfur host should satisfy several essential requirements including high affinity with sulfur to ensure a stable incorporation; high electrical conductivity to fully extract sulfur through electrochemical process; suitable microstructures accessible for the electrolyte to distribute sulfur and trap polysulfides; and a stable framework to sustain the strain generated from volume expansion. Over the years, sulfur cathodes have diversified through microstructure engineering and various materials are involved, including inorganic

compounds, polymers, and carbon materials and their hybrids.

### 2.1. Inorganic Materials

Inorganic materials, such as metal oxides, metal–organic frameworks, and mesoporous molecular sieves, are commonly employed as hosts or additives in cathodes of lithium–sulfur batteries. In the first place, nanosized  $\text{Mg}_{0.6}\text{Ni}_{0.4}\text{O}$  particles were introduced as an additive to acetylene black, a widely-used conducting agent, to remedy its lack of surface area.<sup>[21]</sup> Afterward, the range of nanosized metal oxides particles applied were expanded, to include  $\text{Mg}_{0.8}\text{Cu}_{0.2}\text{O}$ ,  $\text{La}_2\text{O}_3$ ,  $\text{TiO}_2$ , and  $\text{Al}_2\text{O}_3$ , for example.<sup>[22–27]</sup> These nanosized particles, typically 30–50 nm in size, facilitate sulfur utilization by increasing the surface area and suppressing sulfur agglomeration. Moreover, they can trap the produced polysulfides by absorption and to some extent, catalyze sulfur reduction. The introduction of nanosized particles can enhance the delivered capacity and improve the cyclic performances, yet reduce the sulfur content. In many cases, the sulfur content is less than 50 wt%, considering the entire mass of the cathode, which weakens their advantages regarding energy density over conventional lithium–ion batteries.

Technically, inorganic materials are competent as hosts of sulfur. Mesoporous  $\text{TiO}_2$ , with an average specific surface area of ca.  $10^2 \text{ m}^2 \text{ g}^{-1}$ , is reported to impregnate sulfur by a melt-diffusion strategy.<sup>[26,27]</sup> However, limited surface area and pore volume can partially take in a small amount of sulfur, suggesting a quantity of sulfur is spilled. A plausible strategy is confining the sulfur within a hollow chamber. A yolk–shell architecture was developed by Cui and co-workers to overcome the volume expansion.  $\text{TiO}_2$ –S core–shell nanoparticles were first synthesized and partially dissolved by soaking in solution, as shown in **Figure 2a**.<sup>[28]</sup> The empty space was prepared for the volume expansion of sulfur, keeping the  $\text{TiO}_2$  shell intact. This delicately designed structure enabled the battery to be run for 1000 cycles. Succeedingly, a similar structure characterized by a yolk–shell architecture was reported: namely, the inverse opal structure (**Figure 2b**).<sup>[29]</sup> A 3D framework was first prepared through conformally depositing  $\text{TiO}_2$  on polystyrene colloidal particles, then removing the templates. The neighboring polystyrene particles left open channels in the resulting framework, which ensured the infusion of sulfur melt. After annealing in  $\text{H}_2$ , the  $\text{TiO}_2$  framework, primarily in the anatase phase, exhibited an increased conductivity and mechanical strength, making itself eligible as a cathode, without extra conductive agent and binder. The sulfur was

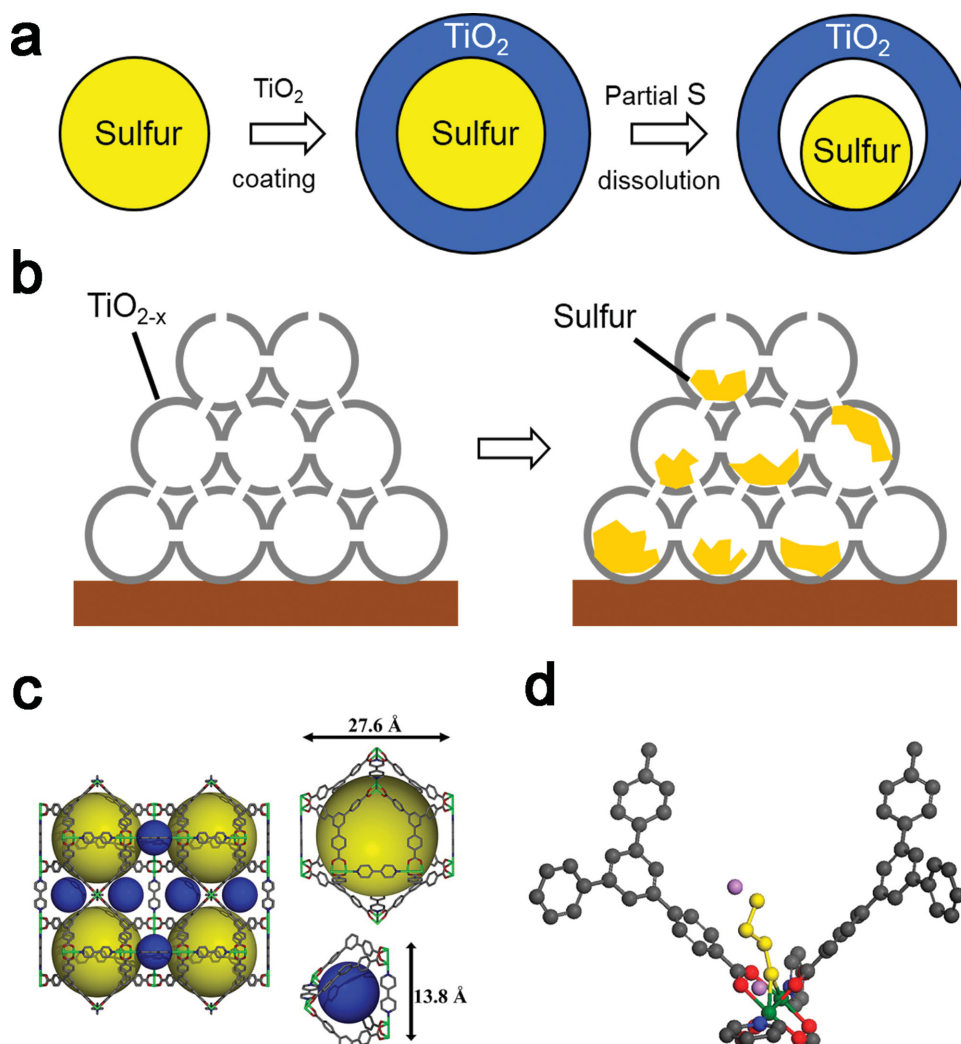


**Figure 2.** Inorganic materials for sulfur cathode. a) Synthesis of S-TiO<sub>2</sub> yolk-shell nanostructured composite particles. Reproduced with permission.<sup>[28]</sup> Copyright 2013, Nature Publishing Group. b) Sulfur cathodes with hydrogen reduced the TiO<sub>2</sub> inverse opal structure. Reproduced with permission.<sup>[29]</sup> Copyright 2014, American Chemical Society. c) Crystal structure of Ni-MOF where the yellow spheres represent mesopores and the blue spheres represent micropores. d) Schematic illustration to the interaction between the polysulfides and the paddle-wheel unit in Ni-MOF. C, O, N, S, Li and Ni atoms are represented by the gray, red, blue, yellow, pink, and green spheres, respectively. Reproduced with permission.<sup>[37]</sup> Copyright 2014, American Chemical Society.

then infiltrated through the open channels, and it partially filled the inner framework, leaving space for volume expansion. Reserving free space for volume expansion, the yolk-shell architecture was inspired by the design of an alloy anode for lithium-ion batteries, which suffers a severe volume expansion, and successfully sequestered the polysulfide within the cathode, realizing a good cyclic performance.<sup>[30]</sup>

Apart from the excellent conductivity, a high surface area is another salient feature that makes porous carbon materials popular as hosts for sulfur. However, this superiority is probably challenged by an appealing material, metal organic frameworks (MOFs), which are renowned for their massive surface area, benefiting from the co-existence of mesopores and micropores. The advantages of MOFs can be summarized into two aspects: the pore-confining effect and host-sulfur interaction. The pore volume delimits the theoretical amount of sulfur imbedded within the cathode, while the surface area influences its distribution. In principle, sulfur

is prone to be well-distributed in the cathode and intimately contact with the conducting substrate, which ensures an utmost use of sulfur. Moreover, the polarized surface of MOF has a strong interaction with the polysulfide, which alleviates the migration of polysulfides. The application of MOFs as electrochemical electrodes has been presented in previous work, revealing that the chemical stability of MOFs, highly dependent on their chemical composition, is critically significant to their electrochemical performance.<sup>[31–33]</sup>

As a creative attempt, MIL-100(Cr), a mesoporous chromium trimesate MOF, was used for encapsulating sulfur and its reduced species in lithium-sulfur batteries.<sup>[34]</sup> The MIL-100(Cr) has a unique architecture comprising two types of mesoporous cages connecting through microporous windows and delivered a comparable surface area with mesoporous carbon. The improved capacity retention indicated that the MIL-100(Cr) outperformed the mesoporous carbon as hosts for sulfur. Similarly, MIL-101(Cr), which has a much larger

surface area up to ca. 5000 m<sup>2</sup> g<sup>-1</sup>, was modified with graphene and used to host sulfur as cathode, and the capacity decay was successfully mitigated.<sup>[35,36]</sup> Besides the spacial confining, the reduced species can be trapped through interactions between sulfur and MOF. For example, Ni<sub>6</sub>(BTB)<sub>4</sub>(BP)<sub>3</sub> (BTB: benzene-1,3,5-tribenzoate; BP: 4,4'-bipyridyl), a Ni-based MOF shown in Figure 2c, can immobilize the polysulfide through coordination between the Lewis acidic Ni(II) and the Lewis base S<sub>x</sub><sup>2-</sup> (Figure 2d).<sup>[37]</sup>

Although it is claimed that the conductivity of the scaffold is less as important as its porosity and surface area, the inorganic materials, indeed, suffer from its inferior conductivity, as exemplified by the low discharge capacity of 689 mA h g<sup>-1</sup>.<sup>[37]</sup> Very recently, a new kind of metal oxide was highlighted because of its metallic conductivity and strong chemical interaction with polysulfides. Ti<sub>4</sub>O<sub>7</sub>, a Magnéli phase titanium oxide, has large amount of low-coordinated titanium atoms that are highly affinitive to polysulfides and has an intrinsic conductivity of 2000 S cm<sup>-1</sup>, which makes it a promising sulfur host. Nazar et al.<sup>[38]</sup> and Cui et al.<sup>[39]</sup> demonstrated the attempts that employ the Ti<sub>4</sub>O<sub>7</sub> in sulfur cathode which is compatible with melt-diffusion composition. The Ti<sub>4</sub>O<sub>7</sub>-S cathode exhibited a decent electrochemical performance. For example, it delivered an initial capacity of 1044 mA h g<sup>-1</sup> that retained by 99% after running for 100 cycles at 0.1 C.<sup>[39]</sup> The high conductivity of Ti<sub>4</sub>O<sub>7</sub> enabled the battery to perform at high rate of 2 C with 70% of capacity survived after 500 cycles.<sup>[38]</sup> The surface coordination of Ti<sub>4</sub>O<sub>7</sub> exerts a strong influence on binding with sulfur species, making Ti<sub>4</sub>O<sub>7</sub> differ from the insulating TiO<sub>2</sub> nanoparticles as physical absorbers and MOFs that rely on acid-base interactions. It was found that the surface interaction between the Ti<sub>4</sub>O<sub>7</sub> and polysulfides allowed controlled and homogeneous deposition of Li<sub>2</sub>S and its reverse oxidation, facilitating the redox electron transfer.<sup>[38]</sup> The importance of surface interaction with polysulfides is highly appreciated by the introduction of Ti<sub>4</sub>O<sub>7</sub> which inspires a new strategy to better the sulfur affinity of the cathode. However, the conductive diluents and binder additives are not exempted entirely thus reducing the sulfur content in the cathode.

## 2.2. Polymers

Electroactive polymers, such as polypyrrole and polyaniline, can undergo charge and discharge processes by redox reactions and have been explored as electrodes in energy storage devices.<sup>[40-44]</sup> In lithium-sulfur batteries, they are usually composited with sulfur in cathodes, not as active materials to store energy, but as supporting substrates to host sulfur and provide conductivity.

In early studies, electroactive polymers were proved to be conducive for enhancing the conductivity and redox kinetics of organic sulfides in rechargeable lithium batteries. In pursuit of high capacities, electroactive polymers are introduced to composite with sulfur to prepare cathodes for lithium-sulfur batteries. The agglomeration and dissolution of sulfur have plagued the early investigation for a long time. A molecular-level composite is expected to decrease

the particle size and suppress the polysulfide migration. To this end, polyacrylonitrile (PAN) was adopted to mix with sulfur and heated at a high temperature (280–300 °C). In that process, the dehydrocyclization of PAN, induced by sulfur, makes the backbone conjugated and conductive. The sulfur, meanwhile, is confined within the pyridine structures of the polymer backbone, in a particle size of less than 10 nm. An initial capacity of 850 mA h g<sup>-1</sup> was presented, which decayed to 600 mA h g<sup>-1</sup> after 50 cycles. The Coulombic efficiency maintained over 95% during cycles.<sup>[45,46]</sup> The performance is considerable at that time and proves that the designed structure is effective in confining the polysulfides, given that a gel electrolyte with LiPF<sub>6</sub> and carbonate, which is reactive with polysulfides, was used.

Polypyrrole (PPy), a conducting polymer, shows a positive effect in lithium-sulfur batteries. Normally, polypyrrole is synthesized by the oxidation of pyrrole monomers, which can be carried out through electropolymerization or chemical polymerization. In preparing the cathode, chemical polymerization is usually preferred by using FeCl<sub>3</sub> and Na<sub>2</sub>S<sub>2</sub>O<sub>3</sub> as oxidant. In the first place, polypyrrole was used as an additive in the cathode to reduce the amount of conductive agent. The conducting PPy was claimed to enhance the conductivity and partially absorb the dissolved polysulfides.<sup>[47]</sup> Moreover, as an electroactive polymer, PPy was reported to denote a capacity of 22 mA h g<sup>-1</sup> in the voltage window of 1.5–3 V. The morphology of PPy has an impact on the performance of batteries. Compared with the granular PPy, the tubular PPy promises a better distribution of sulfur and the staggered arrangement of tubes provide conductive network, which is favorable for long life performance. In fact, tubular PPy indeed outperformed granular PPy in both initial capacity as well as its retention after cycles.<sup>[48,49]</sup> Apart from randomly mixing, the PPy and sulfur can be assembled into a core-shell structure with the aid of a surfactant. For example, micro-sized sulfur particles were synthesized through the disproportionation of sodium thiosulfate induced by p-toluenesulfonic acid, an anionic surfactant. Then, sulfur, pyrrole monomers, and decyltrimethylammonium bromide (DeTAB), a cationic surfactant, were added into an aqueous solution. PPy is believed to nucleate on the sulfur particles, assisted by DeTAB, and then form a layer that engulfs the inner sulfur particle. The core-shell composite benefits from the conducting PPy that providing an effective pathway for both lithium ions and electrons, thus delivered a stable charge-discharge cycles at a relatively high rate.<sup>[50]</sup>

The core-shell structure is a popular strategy to host sulfur and confine polysulfides, which has proved its efficacy in a wide range of cathodes involving different materials. As for polymers, there are many conducting polymers besides PPy to assemble a core-shell structure. For example, polythiophene (PTh) was in situ polymerized on the surface of the sulfur particle as a porous shell.<sup>[51]</sup> Poly(3,4-ethylenedioxythiophene) (PEDOT) was coated around ultrafine sulfur nanoparticles (Figure 3a).<sup>[52]</sup> The conducting-polymer/sulfur composite share the similar benefits. First, the conducting polymer enhances the conductivity and ensures a high sulfur utilization. Second, core-shell particles act as micro-reactors that confine the polysulfides inside and avert

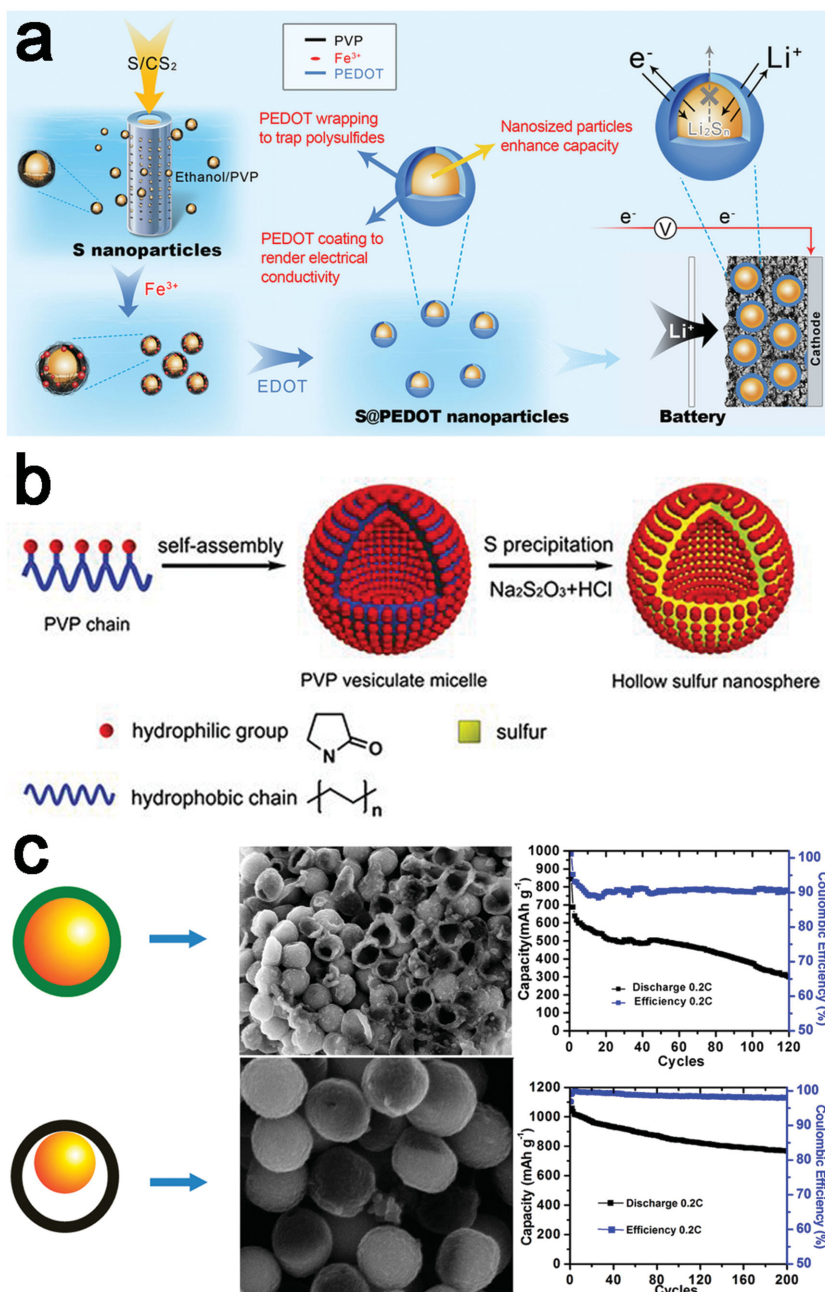


**Figure 3.** Polymers for sulfur cathode. a) Preparation of S-PEDOT core-shell nanoparticles through in situ polymerization. Reproduced with permission.<sup>[52]</sup> Copyright 2013, Nature Publishing Group. b) The formation of PVP encapsulated hollow S nanospheres through self-assembly. Reproduced with permission.<sup>[54]</sup> Copyright 2013, National Academy of Sciences, USA. c) The comparison between the morphologies of S-PANI core-shell and yolk-shell nanoparticles by SEM images after running five cycles and the long-term cycling performance. Reproduced with permission.<sup>[55]</sup> Copyright 2013, American Chemical Society.

the irreversible loss of active materials. In addition, the outer shell can prevent the agglomeration of sulfur particles, thus ensuring a good contact with conducting polymers. These merits are expected to provide a higher capacity and mitigate the capacity decay as reported by Chen et al.: the PEDOT/S core-shell composites exhibited an initial capacity of 1117 mA h g<sup>-1</sup> which was retained at 930 mA h g<sup>-1</sup> after 50 cycles.<sup>[52]</sup>

The core-shell structure can be modified to cope with the volume change during charge and discharge cycles. Therefore a hollow core is preferred, where sufficient space is reserved to buffer the large volume expansion during charge and discharge processes. To this end, a polyaniline (PANI) hollow sphere was synthesized and composited with sulfur by a vapor phase infusion method. The sulfur was claimed to attach on the inner surface of PANI spheres and be trapped by S-C bonds generated in the heat treatment. The resulting composite particles displayed a considerable capacity and cyclic stability, even at high rate up to 5 C. It's noteworthy that the battery was rested in ambient after enduring 500 cycles and then ran another 500 cycles without deterioration in performances. A capacity of 602 mA h g<sup>-1</sup> was retained after 1000 cycles at 0.5 C.<sup>[53]</sup>

The hollow core-shell structure plays a pivotal role to the decent capacity retention while the conducting polymer seems subsidiary, even dispensable. As an example, Cui and co-workers took advantage of the self-assembly of amphiphilic poly(vinylpyrrolidone) (PVP) and sulfur to prepare a vesicular micelle. As the hydrophobic sulfur particles were preferentially grown onto the hydrophobic portion of the PVP, the resulting micelles displayed a typical hollow core-shell structure, where the sulfur was located in the interior of the hollow particle and isolated by the PVP shell (Figure 3b). Although the PVP is nonconductive, the PVP/S composite gave a satisfying capacity of 1018 mA h g<sup>-1</sup> at 0.2 C and a retention of 77.6% after 300 cycles. Further analysis revealed that the sulfur dissolved in the electrolyte was merely 28% of the total sulfur mass after 500 cycles, indicating an effective confinement of polysulfides by the PVP micelles. The particle size after lithiation was slightly changed suggesting that the sulfur expanded inward into the hollow space and the PVP shell was mechanically rigid to stomach the volume change.<sup>[54]</sup>

The yolk-shell structure, another strategy to deal with the volume change, has shown its success in TiO<sub>2</sub>/S composites. Inspired by the former triumph, a PANI/S composite with yolk-shell structure was prepared likewise but in a different method. The interior void was produced from the partial vulcanization with PANI at high temperature to form a cross-linked structure, rather than leaching by solvent. In stark contrast to the core-shell composite, the yolk-shell PANI/S composite displayed an

improved cyclic stability, in line with the former TiO<sub>2</sub>/S composites (Figure 3c).<sup>[55]</sup>

Compared with their competitors, inorganic materials and carbon materials, polymers have no advantage on conductivity and sophisticated architecture. However, their leading superiority is the simple procedure and moderate conditions required for synthesizing, which, moreover, is beneficial to scale up. More conductive than their inorganic competitors, polymers are nonetheless reluctant to make themselves individually serve as cathodes in the absence of conducting agents. Thus, auxiliary conducting agents are often required in preparing the cathode slurry, which inevitably will reduce the sulfur content and thus sacrifice the energy density considering the entire cathode mass.

### 2.3. Carbon Nanomaterials

It is no exaggeration that carbon nanomaterial is the most popular material preferred for sulfur cathodes. It is not only its intrinsic outstanding conductivity, but also its diversity in architecture that make the carbon nanomaterial stand out. Strenuous efforts have been devoted to realize a perfect compositing between sulfur and carbon host, which gives fresh impetus to the burgeoning carbon architectures and results in a vast number of carbon nanomaterials. Nanostructured carbon materials have evolved into several categories which in geometry, can be summed as particles, 1D materials – nanotubes, nanowires and nanofibers, 2D materials – graphene and graphene oxide, and 3D materials such as aerogels and sponges. Moreover, a hierarchical architecture can be obtained by assembling them together.

The diversified carbon materials, like their contenders, polymers and inorganics, are used to host sulfur, provide conductivity and suppress dissolution but seem unrivaled since their salient advantages on conductivity and architectures. Porous structure, large surface area and sufficient pathways, giving access to sulfur's ingress, are favored for cathode. In the following section we will discuss carbon nanomaterials in detail and exemplify the recent progress reported.

#### 2.3.1. Particles

Since the sulfur and its reduction species are electrically isolating which leads to low utilization of sulfur, conducting agents such as carbon black, acetylene black are always required to enable a reversible electrochemical reaction.<sup>[56]</sup> However, the inevitable dissolution and migration of intermediates, higher order polysulfides produced from reactions, has plunged the lithium–sulfur batteries into stagnation. One strategy in response to the tricky issue is using an ionic liquid or polymer gel as the electrolyte to suppress the diffusion, while another relies on porous materials including porous carbon, metal oxides, and conducting polymers to host the sulfur and absorb the dissolved species.<sup>[45,46,57]</sup> However, the inherent drawbacks of low surface area and inferior conductivity lead to a low sulfur loading as well as a large polarization, which reduces the output voltage and energy density.

A breakthrough was made in 2009 when Nazar and co-workers reported a feasible approach toward the theoretical capacity by using highly ordered mesoporous carbon, CMK-3.<sup>[58]</sup> A melt-diffusion strategy was developed for sulfur impregnation since its viscosity is lowest at 155–160 °C and readily to impregnate the channels in the mesoporous carbon driven by capillary forces. The ordered nanostructured carbon framework provided both electrical and ionic pathways but also acted as micro-reactors where the reversible electrochemical reactions underwent and the produced polysulfides were trapped. The resulting battery achieved an unprecedented capacity of 1005 mA h g<sup>-1</sup> at that time. This simple and applicable strategy, introducing nanostructured carbon as sulfur host, paints a promising picture for exploiting the outstanding performances of lithium–sulfur batteries.

In the following years, nanostructured carbon materials diversified by their tailored structure and porosity, spanning from microporous carbon spheres, double-shell hollow carbon spheres, spherical ordered mesoporous carbon, and hollow carbon particles.<sup>[59–63]</sup> For the porous carbon particles, the specific surface area and pore size are the two critical parameters. Liu and co-workers<sup>[64]</sup> and Xiao and co-workers<sup>[65]</sup> investigated a series of porous carbon materials with different pore structures and discussed how pore volume and surface area affect the battery performances. Specifically, the pore volume determines the maximum sulfur loading and accommodates the volume change associated with conversion between sulfur and lithium sulfide, while the surface area has an impact on the distribution of sulfur within the pores. Reviewing several mesoporous carbon materials of different pore sizes, Liu and co-workers found that the pore structure has a slight influence on battery performances provided that the pores are completely filled with sulfur. With pore sizes ranging from 3.4 to 23.1 nm, the capacity nonetheless displayed a small variation, the same as its retention after 50 cycles. It is attributed to the fact that the electrochemical reactions mainly take place at the interface between sulfur and carbon framework. The differences in pore volume are therefore eliminated considering pores are fully filled.<sup>[64]</sup> The large surface area is kinetically favorable for batteries. Normally, sulfur is prone to be well-distributed at a large surface area, which promises a thin coating and intimate contact with the conducting framework. Moreover, during charge and discharge process, especially at high rate, current density is decreased by large surface area, diminishing the polarization and facilitating the conversion. In this regards, high surface area is always preferred for cathode which benefits sulfur utilization, decreases current density and enhances discharge capacity.<sup>[65]</sup>

Promising as porous carbon is, several improvements are still required to deal with the irreversible loss of active materials. For example, CMK-3 was coated with polymers and graphene, which acted as physical barriers to block the egress of polysulfides.<sup>[66–68]</sup> The external coating provides a limited physical interaction to confine sulfur, thus a stronger interaction, like chemical absorption, is preferred. Wang and co-workers synthesized nitrogen-doped mesoporous carbon particles with nitrogen-containing polymer as precursor. The X-ray photoelectron spectrum (XPS) revealed that N

and O atoms were present, besides C atoms. After composing with sulfur, an X-ray absorption near edge structure spectrum was conducted to investigate the local coordination structure around a specific element, which indicated, unexpectedly, that sulfur was bonded with oxygen from carbonyl and carboxyl groups of mesoporous carbon, rather than the doped nitrogen. This conclusion was backed up by the theoretical simulation based on density functional theory. It shows that the nitrogen doping will affect the electronic structure of neighboring oxygen atoms in the carbon matrix thus enhance the chemical interaction between oxygen and sulfur. Compared with those without doping, the nitrogen doped mesoporous carbon exhibited a higher capacity as well as Coulombic efficiency, suggesting that the chemical interaction between sulfur and mesoporous carbon is contributive to a uniform distribution of sulfur, reducing charge transfer resistance and retarding polysulfides diffusion.<sup>[69]</sup>

Nitrogen doping represents a feasible strategy to bind sulfur within the cathode that is introducing heteroatoms into the carbon matrix. However, it is not always as effective to enhance battery performance as doping nitrogen. As reported by Sun and co-workers, introducing oxygen functional groups poses a negative effect of reduced conductivity and unwanted side reactions between sulfur and oxygen species, which lead to a deterioration in performance.<sup>[70]</sup> These results seem conflicting to Wang's conclusion that attributes the benefits of nitrogen doping to the enhancement of the sulfur–oxygen interaction. The contradiction has not been resolved yet, reflecting the fact that the interaction between sulfur and its host is complicated, and more discussions are needed.

As sulfur can react transition metals to form metal sulfides, another chemical interaction is expected between sulfur and metal decorated carbon matrix. Wang and co-workers took advantage of the bonding between sulfur and copper to stabilize active materials within microporous carbon host.<sup>[71]</sup> Copper particles were incorporated within the microporous carbon by an ultrasonic-assisted wetness impregnation and synchro-dry technique. The authors have claimed there is a chemical bonding between sulfur and copper, as verified by X-ray photoelectron spectroscopy and X-ray diffraction analysis. The effect of copper stabilization was prominent in carbonate-based electrolyte, which is prone to react with dissolved polysulfides. The discharge voltage profile did not display the normal two-plateau shape. Instead, it exhibited only one plateau at 1.5 V, which is similar in shape but lower in voltage compared with those performed in carbonate-based electrolyte.<sup>[46,59,72]</sup> The battery's cyclic performance, in stark contrast to the bare one, was much improved: the capacity steadily retained above 600 mA h g<sup>-1</sup> over 500 cycles.

The microporous carbon was reported to have a space confinement effect that metastable small sulfur allotropes S<sub>2-4</sub> were formed within the micropores (<0.5 nm) of the carbon host.<sup>[73]</sup> The small sulfur promised a better performance than the capacity stayed 1149 mA h g<sup>-1</sup> over 200 cycles even at a carbonate based electrolyte. A sketchy explanation was presented that the high order polysulfides were avoided due to space confinement. But there are more

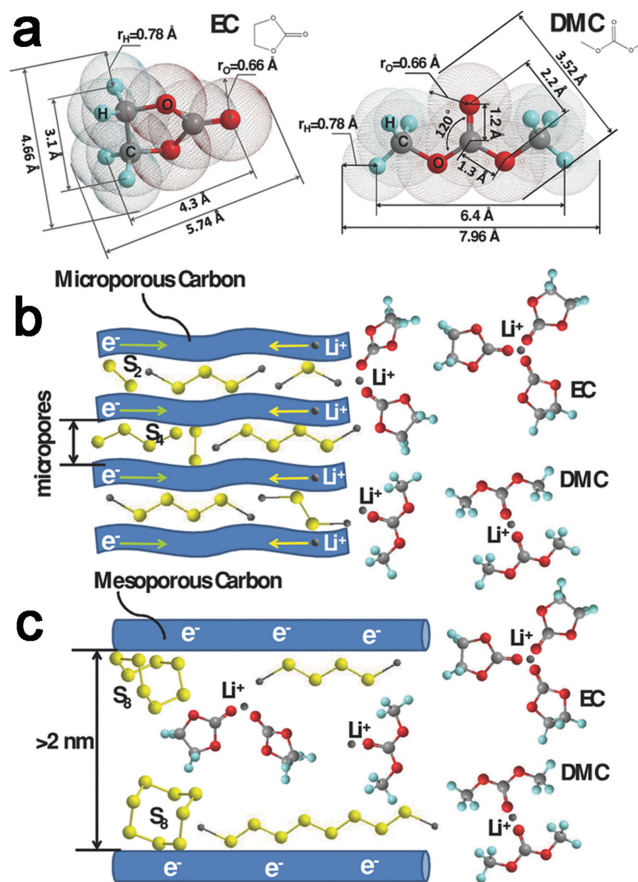


**Figure 4.** Porous particles for sulfur cathode. a) Theoretical calculation of the dimensions of ethylene carbonate and dimethyl carbonate molecules. b,c) Schematic illustration of the lithiation of sulfur in microporous carbon (b) and mesoporous carbon (c) in carbonate-based electrolyte. Reproduced with permission.<sup>[74]</sup> Copyright 2014, Wiley-VCH.

questions awaiting answers including the unique electrochemical behavior as well as the compatibility to carbonate based electrolyte. Recently, more details were unveiled on these issues. Huang et al. demonstrates via theoretical calculation that the carbonate molecules, like ethylene carbonate (EC) and dimethyl carbonate (DMC), whose geometric dimensions are larger than the size of microporous carbon, are prevented from access to sulfur molecules by physical barrier (**Figure 4**).<sup>[74]</sup> Hence, the battery with microporous carbon can well perform in the carbonate based electrolyte rather than deteriorate due to irreversible reaction between carbonate and polysulfide. They also proposed a solid–solid mechanism to describe the lithiation–delithiation reaction of S<sub>2-4</sub> confined in microporous carbon, which overcame higher kinetic resistances and rendered the lowered discharge plateau. The microstructure carbon matrix makes the battery immune from the carbonate species and imparts a good adaptability to the electrolyte. However, the microporous carbon is also inherited with shortcomings that the output voltage is relatively lower and the sulfur content confined within the micropores is limited, which sacrifices the energy density of the battery. To this end, a combination of micropores and mesopores in carbon hosts can benefit for a better performance. Huang et al. have demonstrated

a core-shell carbon particle as the sulfur host where highly ordered mesoporous carbon is in the core to take in sufficient sulfur and microporous carbon at the shell serves as physical barrier to stabilize sulfur cathode. The sulfur loading in the host particle, as a result, was increased to more than 60% and the capacity retained 80% after 200 cycles, indicating a synergistic advantage of both micropore and mesopore.<sup>[75]</sup>

### 2.3.2. 1D Carbon Materials

1D carbon materials, including carbon nanofibers and nanotubes, are widely used in energy devices, including solar cells, supercapacitors and lithium-ion batteries, benefitting from their superiority in high electrical conductivity, mechanical strength, and surface area.<sup>[1,2,76–80]</sup> They also show their advantages in lithium-sulfur batteries. Distinct from porous carbon particles, the carbon materials discussed in this section have a large aspect ratio that endow them with sufficient surface, both internal and external, to affix sulfur, as well as efficient pathway for electrons. More importantly, 1D carbon materials can assemble into a conducting network where nanofibers or nanotubes interpenetrate each other, thus make the cathode free-standing without binder or conducting agent, which is beneficial for flexible cathode.<sup>[81–85]</sup>

A commercially available active carbon cloth was first used to host sulfur as a binder-free cathode.<sup>[81]</sup> The carbon cloth comprises carbon filaments with micropores where sulfur was impregnated. Although a capacity of  $1057 \text{ mA h g}^{-1}$  was delivered which retained by 75.7% after 80 cycles, the micropores (<2 nm) did not provide adequate volume for sulfur resulting in a low sulfur content of 33%. In this case, the original intention to prepare a binder free cathode that enabling the battery a higher sulfur content, which promises a larger energy density considering the entire cathode, is worn off. Creating pores on the surface is probably helpful to resolve the problem. Zhang and co-workers synthesized porous carbon nanofiber with polyacrylonitrile (PAN) and poly(methyl methacrylate) (PMMA) but it does not seem very encouraging since the sulfur content of the cathode is still lower than 30%.<sup>[86]</sup> In this case, carbon nanotubes or hollow carbon nanofibers are more eligible as sulfur host because sulfur can be impregnated in the inner space. Wang's group and Cui's group have made efforts to encapsulate sulfur within the hollow carbon nanofibers.<sup>[87,88]</sup> Prepared from anodic aluminum oxide template, the hollow carbon nanofibers, whose diameter is within 200–300 nm, are favorable for sulfur filling. The sulfur content in the cathode, without binder or conducting additives, can reach up to 75%.<sup>[88]</sup> However, Cui and co-workers found that  $\text{Li}_2\text{S}_x$  detached from carbon matrix after lithiation and further investigation by first-principles calculations revealed a dramatic decrease of binding energy between  $\text{Li}_2\text{S}_x$  and carbon matrix. It is concluded that the lithiation during discharge process leads to changes in chemical interaction between sulfur and carbon, which is attributable to the capacity fading. In light of the understanding that the interfacial effect played an important role in cyclic performance, they introduced amphiphilic polymers, poly(vinylpyrrolidone) (PVP) and Triton X-100, to modify the carbon surface.<sup>[89]</sup> The chemical

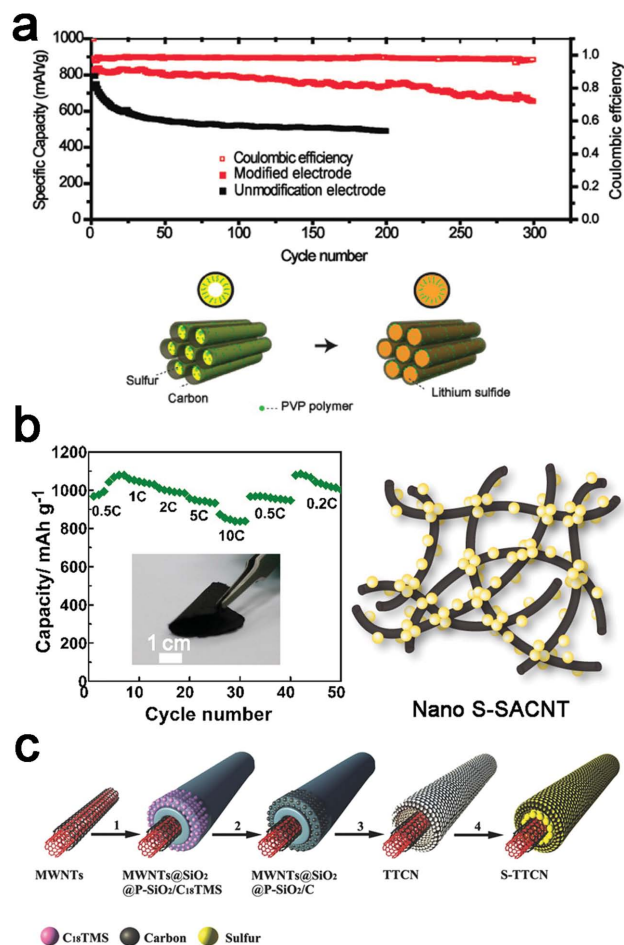


**Figure 5.** 1D carbon materials for sulfur cathode. a) Schematic illustration to sulfur cathode with the amphiphilic surface-modified hollow carbon nanofibers and the improved cyclic performance of the battery. Reproduced with permission.<sup>[89]</sup> Copyright 2013, American Chemical Society. b) Schematic illustration and optical image of the binder-free cathode with sulfur nanocrystals confined in carbon nanotube networks and the rate performance of the resulting battery. Reproduced with permission.<sup>[84]</sup> Copyright 2014, American Chemical Society. c) Preparation of the porous carbon-nanotubes-sulfur composite. Reproduced with permission.<sup>[94]</sup> Copyright 2014, Wiley-VCH.

moieties of amphiphilic polymer acted as anchoring points to make polar  $\text{Li}_2\text{S}_x$  strongly bind with nonpolar carbon matrix, thus immobilize the discharge products. The polymer modified cathode delivered a specific capacity of  $1180 \text{ mA h g}^{-1}$  at 0.2 C and a capacity retention of 80% over 300 cycles at 0.5 C, much improved compared with former results, a capacity retention of 48.5% after 150 cycles at 0.5 C (Figure 5a).<sup>[88]</sup>

In comparison, carbon nanotubes have much smaller diameter of 10–20 nm so that sulfur is reluctant to infiltrate into the tubes. Therefore, as for cathodes using carbon nanotubes, sulfur is usually affixed around the surface and the mutual interaction can be enhanced by introducing heteroatoms like N and O in the carbon nanotubes.<sup>[90,91]</sup> For example, Manthiram and co-workers deposited sulfur on the carbon nanotubes that were intertwined into a self-standing film.<sup>[85]</sup> Surprisingly, this composite cathode can deliver a capacity of  $1352 \text{ mA h g}^{-1}$  at a high current rate of 1 C which maintained  $915 \text{ mA h g}^{-1}$  after 100 cycles. The impressive rate

performances should be attributed to the 1D configuration of the carbon nanotubes that have large surface area for sulfur loading, but also are interlaced to provide sufficient conducting pathways with lower interfacial contacting resistance. The average energy density over 100 cycles based on the cathode was calculated as  $852 \text{ W h kg}^{-1}$  with sulfur content of 40 wt%. In contrast, the carbon black/sulfur composite with the same sulfur content showed an inferior performance, which highlights the benefits of carbon nanotubes. Liu and co-workers reported a similar carbon nanotube/sulfur composite film but with a higher sulfur content of 65 wt%.<sup>[83]</sup> It should be mentioned that the carbon nanotubes were pre-oxidized in the  $\text{HNO}_3/\text{H}_2\text{SO}_4$  mixture to reinforce the carbon–sulfur interaction. In line with the former results, the as-prepared cathode demonstrated a decent rate performance and an energy density of  $1200 \text{ W h kg}^{-1}$  over 100 cycles at 0.1 C, which is rarely achieved by conventional sulfur cathodes. Wei and co-workers employed aligned carbon nanotubes as interconnected conductive scaffolds to accommodate sulfur with high sulfur content of 90 wt%, rendering a dramatic increase in energy density and power density.<sup>[92]</sup> Apart from coating along the carbon nanotubes, sulfur can also be anchored on the outer surface in the form of nanoparticles. Wang and co-workers deposited sulfur nanocrystals conformally along the outer surface of super aligned carbon nanotubes through a solution based process.<sup>[84]</sup> As the carbon nanotube network prevents the agglomeration of sulfur, resulting in the sulfur nanocrystals anchoring on the carbon nanotubes with a grain size of 10–20 nm, more surface was exposed in the electrolyte which favors the utility of sulfur. Consequentially  $909 \text{ mA h g}^{-1}$ , 85% of initial capacity, retained after 100 cycles at 1 C (Figure 5b).

Having a large aspect ratio, however, the surface area of carbon nanotubes, reported to be around  $100 \text{ m}^2 \text{ g}^{-1}$ , is still dwarfed by that of porous carbon particles.<sup>[83]</sup> Therefore, attempts to increase the porosity on the carbon nanotube are motivated. One approach is to introduce defects. Huang and co-workers designed a water steam etching method to create porous carbon nanotubes.<sup>[93]</sup> Through the chemical reaction with oxygen from water stream at high temperatures, the resulting carbon nanotubes have a larger surface area, up to  $431.2 \text{ m}^2 \text{ g}^{-1}$ , an increase of several folds. At the same time, the structural integrity and electrical conductivity are well maintained. The cathode with increased porosity enables a high sulfur content up to 70%. This high sulfur loading, however, did not lead to a performance degradation, as it usually does. An initial capacity of  $1382 \text{ mA h g}^{-1}$  was recorded and it retained to  $950 \text{ mA h g}^{-1}$  after 250 cycles at 0.2 C. Even at a high current rate of 5 C, the battery delivered a  $455 \text{ mA h g}^{-1}$  after 250 cycles, corresponding to 70% capacity retention.

Another approach seems more complicated. It intends to combine conducting carbon nanotubes with porous carbons to obtain a hybrid. The conventional strategy is to coat a porous carbon layer around the carbon nanotubes resulting in a core-sheath structure, which contains precursor coating and calcination. Guo and co-workers used this method to coat a microporous carbon around the carbon nanotubes.<sup>[73]</sup> The microporous carbon have a spatial confining effect to

make the sulfur filled transform into small sulfur allotropes. The details have been discussed previously but it should be mentioned that the surface area is dramatically increased to  $936 \text{ m}^2 \text{ g}^{-1}$ , indicating the efficacy of this method. Recently, Guan and co-workers report a novel tube-in-tube structured carbon nanomaterial as the host for sulfur cathode.<sup>[94]</sup> Acid-treated carbon nanotubes were first coated with porous  $\text{SiO}_2$  layers, then an organosilicon compound was added as the porogen agent and carbon precursor, which was converted into carbon after chemical treatment and high temperature calcinations. Next, the  $\text{SiO}_2$  layer was etched away to form the product with carbon nanotubes confined within hollow porous carbon nanotubes (Figure 5c). The surface area was increased to  $822.8 \text{ m}^2 \text{ g}^{-1}$  due to the introduction of porous layer. The 1D carbon nanotubes provided remarkable electrical conductivity and the porous carbon layers retarded the diffusion of polysulfides, giving a considerable capacity of  $1274 \text{ mA h g}^{-1}$  and a stable cycling retention of 72% after 50 cycles. More importantly, the large pore volume enable the cathode to host more sulfur improving the energy density of batteries. Yet the cathode was not rid of conducting additives and binder completely, rendering a sulfur content of 56 wt%.

Compared with porous carbon materials, the 1D carbon materials have less pores and lower surface area. Nevertheless, these drawbacks are made up by several merits: First, the 1D configuration favors electronic and ionic transport, making them eligible as conducting pathways and free from conducting agents. Second, the carbon nanofibers or nanotubes with large aspect ratio are apt to intertwine in the network, endowing the cathode with rigidity and flexibility and making it self-standing and free from binders. Third, the inner space of hollow fiber or the surface of carbon nanotubes provide adequate space to host sulfur and accommodate the volume expansion. Fourth, 1D carbon materials are readily to acquire, some of which are even commercialized.

### 2.3.3. 2D Carbon Materials

Graphene, as a typical and the most arresting 2D material, who has superior electrical conductivity, high surface area (ca.  $2600 \text{ m}^2 \text{ g}^{-1}$ ), and structural stability, has been proved favorable for electron or hole transfer over its basal plane.<sup>[95]</sup> Moreover, recent reports show that graphene can be assembled into different macro-assemblies including fibers, membranes and aerogels.<sup>[96–98]</sup> The excellent properties and structural diversity make graphene popular as electrode material in energy devices.<sup>[99–101]</sup> So it does in lithium–sulfur batteries. Naturally, the large surface area of graphene can be used to coat the sulfur particle as a physical barrier to provide conductivity, trap polysulfide and prevent agglomeration, but this strategy is not as successful as expected. A poly(ethylene glycol) (PEG) modified sulfur wrapped by graphene has been proved more effective by Cui and co-workers.<sup>[102]</sup> The PEG on the sulfur particles provided a flexible cushion between the sulfur and the graphene sheet to buffer the stress and volume changes. Moreover, PEG chains associated with the graphene sheet were capable of retarding the diffusion of polysulfides. Therefore, the composite cathode delivered a stable capacity over  $600 \text{ mA h g}^{-1}$  at 0.2 C. Afterward, the

core-shell structure was modified by using reduced graphene oxide to encapsulate sulfur.<sup>[103]</sup> The capacity stabilized above 500 mA h g<sup>-1</sup> over 500 cycles at a high rate of 3 C. In addition, the sulfur content in the composite increased to 83% and it is beyond 65% considering the extra conducting agent and binder in the cathode. Zhou and co-workers devised a simpler approach to wrap graphene oxide around sulfur through solution ionic strength engineering.<sup>[104]</sup> Instead of melt-diffusion and chemical deposition, they composite sulfur and graphene oxide in a physical way which takes advantage of the fact that graphene oxide is apt to crumple and wrinkle to minimize its surface energy when dispersed in ionic solutions. When sulfur particles, regardless of their sizes, are added in ionic solutions, driven by reducing the surface energy, graphene oxide is prone to wrap the sulfur particles and precipitate, rendering a core-shell structure. Moreover, the thickness of graphene oxide can be readily tuned by adjusting the weight ratio of sulfur and graphene. The space between the graphene oxide layers provides channels for lithium ions and impedes polysulfides diffusion. The result is encouraging. The core-shell structured sulfur-graphene oxide cathode enabled the battery to endure 1000 repeated charge-discharge cycles. The capacity after 1000 cycles at 0.6 C was 800 mA h g<sup>-1</sup>, indicating a retention of 89%. The extraordinary cyclic performance declared success of this simple method based on solution ionic strength engineering. However, it should be noted that graphene oxide is a bad conductor and sulfur tends to agglomerate in solution, so the conducting additive is indispensable in the cathode.

Benefitting from the 2D configuration, graphene oxide provides an adequate surface area to sulfur, where the functional groups, epoxy and hydroxyl groups, are conducive to anchoring the sulfur, and the pores or cavities can intimately contact with the sulfur to ensure conductivity and prevent aggregation. For example, Zhang and co-workers deposited sulfur on the graphene oxide sheets through a chemical method.<sup>[105]</sup> Over 50 cycles at 0.1 C, the capacity maintained well around 950 mA h g<sup>-1</sup> though enduring a capacity drop at first few cycles. Regrettably, however, considering the inferior conductivity of the graphene oxide, 20% of conducting agent is still necessary. To further immobilize sulfur, graphene is modified by introducing chemical agents or incorporating with polymers. Zu and Manthiram found that the hydroxylated graphene nanosheet showed a better cyclic stability and rate performances, which was attributed to the evenly distributed hydroxyl groups.<sup>[106]</sup> Wang and co-workers introduced ferric chloride (FeCl<sub>3</sub>) as an oxidizing agent as well as a soft template to obtain a uniform sulfur deposition on graphene.<sup>[107]</sup> Yang and co-workers reported a pollutant control strategy by reducing the graphene oxide with hydrogen sulfide (H<sub>2</sub>S).<sup>[108]</sup> The reduction process resulted in a graphene-sulfur composite where sulfur was well-distributed over the curly wrinkle graphene layers. Polymer with functional groups and unique chain structure can not only confine polysulfides through chemical interactions but also buffer volume expansion and prevent pulverization. Polydopamine was used as a soft buffer layer to crosslink with binder and graphene-sulfur composites. The cathode was hence stabilized for long-term charge-discharge cycles.<sup>[109]</sup> Amylopectin,

a natural polymer which has a plenty of hydroxyl groups, is expected to interact with hydroxyl groups on graphene oxide through hydrogen bonds.<sup>[110]</sup> Therefore, the graphene oxide layers were cross-linked into a 3D structure, helpful to tether the polysulfides. Similarly, a cationic surfactant, cetyltrimethyl ammonium bromide (CTAB), was used to modify the sulfur coated on the graphene oxide sheet.<sup>[111]</sup> With the help of CTAB, sulfur is uniformly strewn over graphene oxide without agglomeration. An initial capacity of 1440 mA h g<sup>-1</sup> was recorded at a current rate of 0.2 C. A package of strategy was adopted to enhance the cyclic performance including elastomeric binders, ionic liquid electrolyte and CTAB modified graphene oxide-sulfur cathode. The repeated charge-discharge at 0.05 C was prolonged to an unprecedented 1500 cycles with capacity of 700 mA h g<sup>-1</sup> remained. Moreover, the battery exhibited a decent rate performance. For example, it left 800 mA h g<sup>-1</sup> at a high rate of 6 C after 150 cycles. The graphene oxide/sulfur composite has a high sulfur content of 80% thus ensuring 56 wt% of sulfur in electrode, despite the fact that 20% of conducting agent was added.

Besides chemical modification, very recently, Zhang et al. reported a nitrogen-doped graphene as sulfur cathode.<sup>[112]</sup> The native morphology of the N-doped graphene sheets with crumples and wrinkles provides abundant cavities for sulfur loading, and the strong ionic attractions between the nitrogen and the lithium exert a considerable impact on the diffusion and redistribution of the lithium-sulfur compound. The cycle life of the resulting battery was significantly prolonged to 2000 cycles with capacity of 347 mA h g<sup>-1</sup> retained at 2 C.

The theoretical surface area of graphene is 2630 m<sup>2</sup> g<sup>-1</sup>.<sup>[95]</sup> However, the reality is not always as encouraging as it looks. It is reported that the reduced graphene oxide possessed a surface area of 106 m<sup>2</sup> g<sup>-1</sup>, in stark contrast to its theoretical value.<sup>[113]</sup> In fact, the graphene is annoyed by its small surface area arising from their strong  $\pi$ - $\pi$  stacking. Therefore, several attempts at nanostructure engineering of the graphene to increase its surface area have been carried out. For example, Zhang and co-workers created nanopores on graphene sheets through chemical activation of KOH.<sup>[113]</sup> Huang and co-workers exfoliated graphite through a micromechanical method assisted by sulfur.<sup>[114]</sup> With the same intention to increase the porosity of the graphene materials, like one has done for carbon nanotubes described before, Chen et al. designed a hybrid architecture that composite porous carbon with graphene layers.<sup>[115]</sup> This hybrid architecture is aiming at separating the sulfur reservoir and current collector, which are functioned by porous carbon and graphene layer respectively (**Figure 6a**). The porous carbon was activated from the phenolic resin, the precursor that was polymerized on the surface of graphene, and uniformly covered the surface of graphene layer. The surface area and pore volume were evidently raised to 2500 m<sup>2</sup> g<sup>-1</sup> and 1.94 cm<sup>3</sup> g<sup>-1</sup> and a higher content of sulfur, 61.2 wt%, was taken in. Recently, Wei's group reported a novel strategy to figure out the stacking of graphene layers. Based on the fact that the graphene would be hard to stack should it contains a great deal of protuberances, they had epitaxially grown graphene with intrinsic protuberances on a mesoporous template (**Figure 6b**).<sup>[116]</sup> The obtained template graphene of two unstacked graphene layers separated by

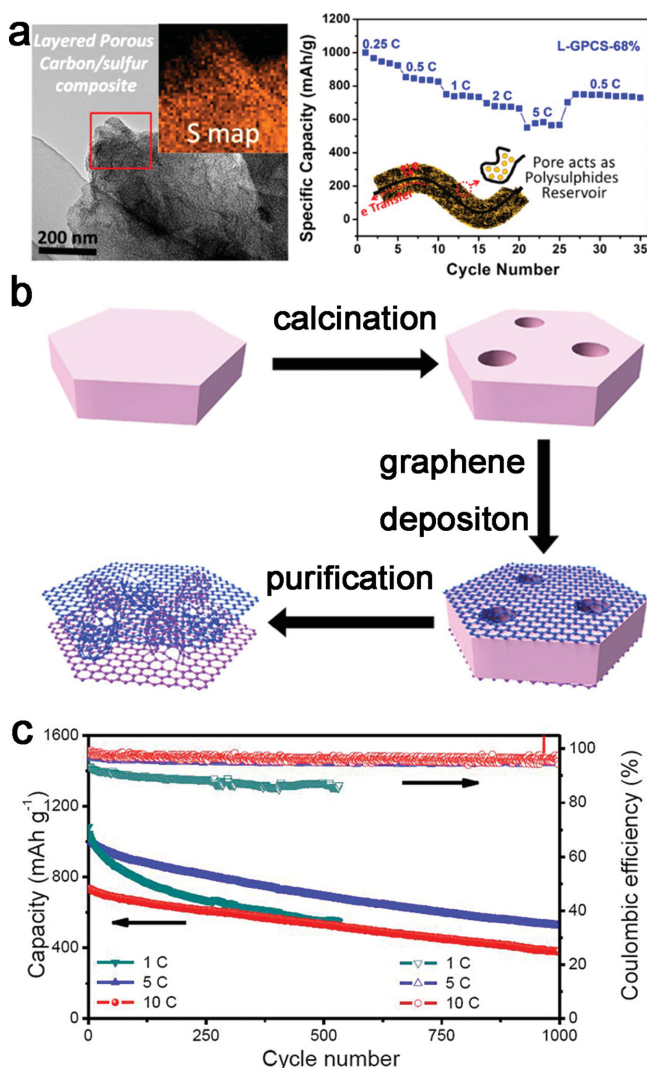


**Figure 6.** 2D carbon materials for sulfur cathode. a) SEM image and sulfur mapping of the graphene-based sulfur cathode and the rate performance of the battery. Reproduced with permission.<sup>[115]</sup> Copyright 2014, American Chemical Society. b) Preparation of the unstacked double-layer template graphene. c) The cyclic performance of the resulting battery. Reproduced with permission.<sup>[116]</sup> Copyright 2014, Nature Publishing Group.

protuberances was endowed with large surface area of  $1628 \text{ m}^2 \text{ g}^{-1}$  and high electrical conductivity of  $438 \text{ S cm}^{-1}$ , which made it competent as sulfur host and immune from the conducting agent. The protuberances and the interlayer space are both available for sulfur leading to a sulfur loading of 64 wt% in the composite. As we presented previously, the carbon framework with large surface area can undermine the current density through the cathode whilst guaranteeing a high utility of active materials, thus making the battery more adaptable to high rate charge–discharge process,<sup>[65]</sup> so it is satisfying that the final performance was in line with the above assertion. At a high rate of 5 C, the battery delivered a high capacity of  $1034 \text{ mA h g}^{-1}$ , and it was maintained at around half that after 1000 cycles. Even at a higher rate of 10 C, the battery also work normally and after undergoing 1000 cycles, more than 50% of capacity still left (Figure 6c).

Apart from a few examples that use carbonized eggshell membranes or MOF-derived carbon as carbon frameworks for sulfur cathode, in most cases, graphene materials take the dominant position in 2D materials.<sup>[117,118]</sup> Benefiting from its planar shape, graphene is suitable as a physical barrier to coat around sulfur particles. Also, the decent conductivity enables graphene, sometimes assisted by additives, to be a framework to host sulfur. After modification, sulfur can be uniformly spread over the entire plane of graphene. The chemical moieties scattered on the graphene sheets will interact with polysulfides and the wrinkles and crumples of the graphene sheet can form voids and cavities to block their diffusion. Thus, graphene materials can rival porous particles or 1D materials in sulfur cathodes. Moreover, considering the pore-less structure, sulfur is usually composited with graphene through chemical deposition from metallic sulfide, which is favorable for a higher sulfur loading than the conventional melt-diffusion method.

### 2.3.4. 3D Carbon Materials

Carbon aerogels, sponges, foams, and frameworks are typical 3D carbon materials that are also favorable in lithium batteries. In many cases, they are assembled from either carbon nanotubes or graphene units forming integral and stable framework.<sup>[119]</sup> For example, carbon nanotubes can assemble into a cage enclosing bi-pyramidal sulfur particles.<sup>[120]</sup> Compared with the former described core–shell structure, the carbon nanotube cage here has a larger size, up to  $20 \mu\text{m}$  and affords 35 vol% buffer space for volume expansion; besides, 3D hyper-branched hollow carbon nanorod was prepared from MgO template.<sup>[121]</sup> Sulfur was encapsulated into the hollow branch of the framework which is sequestered from the electrolyte (Figure 7a). The hyper-branched hollow carbon nanorod with high aspect ratio and junctions can effectively retard the diffusion of polysulfides and diminish the shuttle effect. Moreover, the 1D carbon branch is kinetically favorable for electron transportation contributing to remarkable rate capability and cyclic stability (Figure 7b and 7c). As a demonstration, it delivered an initial capacity of  $1255 \text{ mA h g}^{-1}$  at 0.5 C and retained 91.4% after 500 cycles. At a higher rate of 10 C, the cathode still afforded a capacity of  $663 \text{ mA h g}^{-1}$  and a retention of 85.6% after 500 cycles.

Self-standing carbon sponges were synthesized from graphene through a hydrothermal reaction.<sup>[122]</sup> With a conductivity of  $42 \text{ S m}^{-1}$  and surface area of  $215 \text{ m}^2 \text{ g}^{-1}$ , the graphene sponges displayed decent properties eligible to reserve sulfur and immune from conducting agents and binders. It is of more importance that the 3D architecture afforded a high areal specific capacity and retention at a large sulfur loading of  $12 \text{ mg cm}^{-2}$ . The previous report illustrates that charge transport in nitrogen-doped graphene is enhanced since graphitic nitrogen donates mobile electrons to the graphene conducting band.<sup>[123]</sup> Accordingly, a 3D nitrogen-doped graphene foam was used as framework in sulfur cathode (Figure 7d). Prepared from a solvothermal process, the N-doped graphene foam, with higher surface area ( $398 \text{ m}^2 \text{ g}^{-1}$ ) and conductivity ( $102 \text{ S m}^{-1}$ ), showed stronger interaction with sulfur through chemical bonding as verified by X-ray

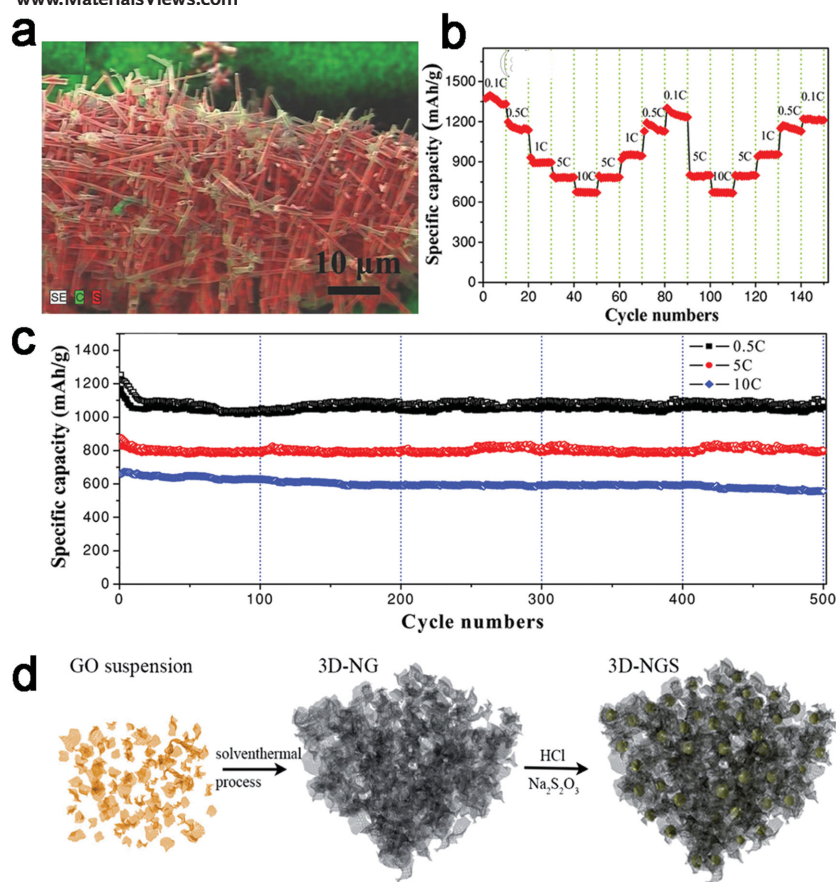


**Figure 7.** 3D carbon materials for sulfur cathode. a) SEM elemental mapping image of sulfur cathode with hyperbranched hollow carbon nanorod architectures. b,c) The rate and cyclic performance of the resulting battery. Reproduced with permission.<sup>[121]</sup> Copyright 2014, Wiley-VCH. d) Preparation of 3D nitrogen-doped graphene cathode. Reproduced with permission.<sup>[124]</sup> Copyright 2014, Royal Society of Chemistry.

photoelectron spectroscopy.<sup>[124]</sup> Consequently, a capacity of  $792 \text{ mA h g}^{-1}$  was retained, indicating the retention of 92.5% after 145 cycles at a current density of  $600 \text{ mA g}^{-1}$ . Shen and co-workers prepared a 3D graphene-like material with hierarchical pores based on ion-exchange resin. The abundant micro- and mesosized pores provide an exceptionally high surface area of  $2700 \text{ m}^2 \text{ g}^{-1}$  and large pore volume of  $2.5 \text{ cm}^3 \text{ g}^{-1}$  capable of a large sulfur loading. The 3D structures in the carbon framework with pores interconnecting and conjoining provide sufficient surfaces and channels for sulfur infusion and access for lithium-ion transportation. Meanwhile, the volume expansion is to be accommodated by the hierarchical architecture so that sulfur is enclosed in the carbon framework, which also, is conductive enough to facilitate the thorough conversion of sulfur.<sup>[125]</sup> As a result, the 3D nanocomposite delivered a capacity up to  $1067 \text{ mA h g}^{-1}$  of which 84.5% is retained after 300 cycles at 0.5 C.

## 2.4. Hybrid Materials

The cathode in lithium–sulfur batteries always has a bespoke structure: conducting electrons, storing sulfur, and trapping polysulfides. For those host materials in the past, spanning

from polymers, metal oxides and carbon materials, their intrinsic properties can hardly satisfy all the requirements for a high-performance sulfur cathode. It is well-reasoned, therefore, that we can integrate the merits of an individual component pursuing a synergetic effect in a hybrid material. Generally, porous carbon or 1D carbon materials are endowed with an adequate surface area, but have limited effect in confining the active materials. In response, introducing another component, like polymers or graphene, as a physical barrier can be beneficial to moderate the capacity fading.<sup>[66–68,126–128]</sup> Recently, Liu's group significantly improved the cyclic stability by coaxially wrapping graphene over sulfur-coated carbon nanofibers.<sup>[129]</sup> At a rate of 1 C, the battery exhibited a rather slow capacity decay, 0.043% per cycle over 1500 cycles. The graphene was coated on the carbon nanofibers through a pH-adjusting process, taking advantage of the difference in their zeta-potentials. It should be noticed that the capacity slumped in the first few cycles and stabilized afterward, revealing that the polysulfides still partially diffused and then saturated the electrolyte. The loose cohesion between graphene and carbon nanofiber was to blame. In this regard, an intimate coating shell was achieved through in situ polymerization of pyrrole on the surface of carbon nanotubes.<sup>[126]</sup>

Compared with nanofibers, carbon nanotubes have a much smaller diameter and a higher surface area, which is beneficial for sulfur loading. As reported by Amine and co-workers, sulfur was coated outside the carbon nanotube through a thermal infusion process, then the composite was sandwiched within interlayer galleries of graphene.<sup>[130]</sup> The hierarchical sandwich-type architecture took advantage of the carbon nanotube to make sulfur well-distributed and prevent the unwanted restacking of graphene. Moreover, the graphene layer separated the cathode into small chambers for electrochemical reaction meanwhile providing channels for lithium ions. The sulfur content in the cathode was raised to 49%, in comparison with the 33% reported in the case of carbon nanofibers.<sup>[129]</sup>

The above-mentioned hybrid materials, in most cases, were prepared by physical mixing, which brings about the inevitable contact resistance between the components, like carbon nanotube and graphene. From another perspective, these  $\text{sp}^2$ -hybridized carbon materials are prone to stack together, thus reducing the surface area accessible for ions and space available for sulfur loading. To this end, a targeted strategy that covalently integrates the carbon nanotubes and graphene into a hierarchical architecture can be conducive to exploiting the properties of individual component.<sup>[101]</sup> As shown in **Figure 8a**, graphene/single-walled carbon

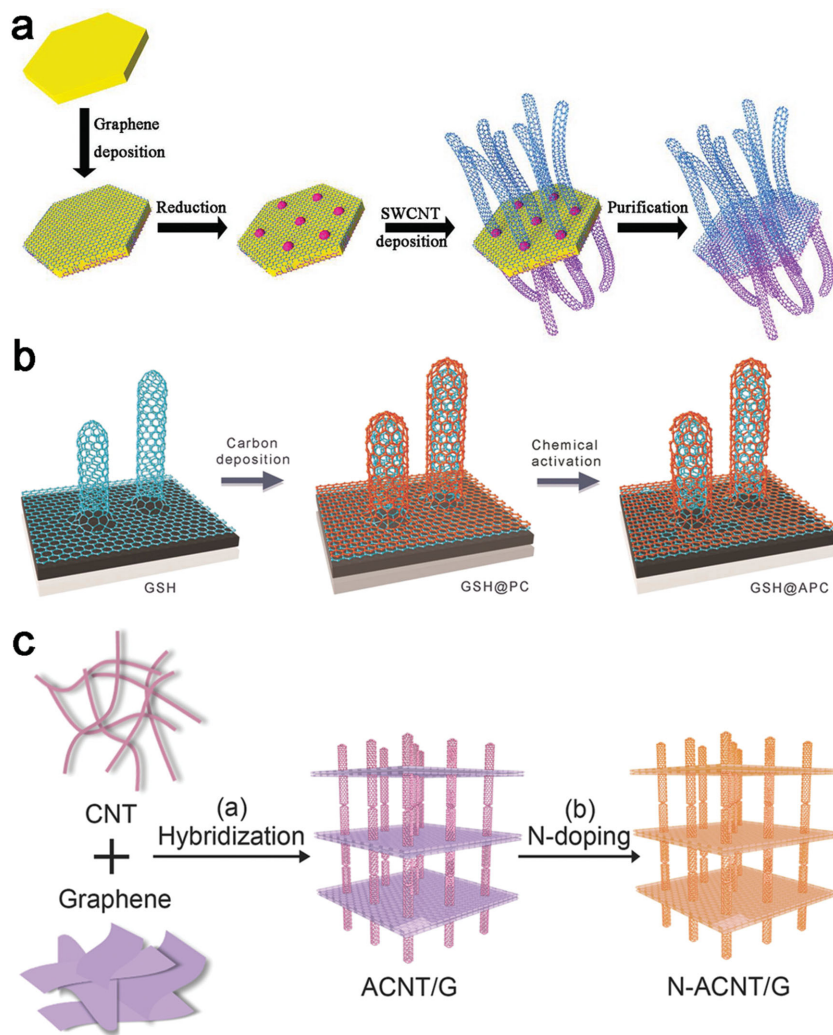


**Figure 8.** Hybrid materials for sulfur cathode. a) Preparation of graphene–single-walled carbon nanotube hybrid materials through a template-based chemical vapor deposition process. Reproduced with permission.<sup>[131]</sup> Copyright 2012, American Chemical Society. b) Preparation of nanoarchitected graphene–carbon nanotube and porous carbon hybrid materials. Reproduced with permission.<sup>[132]</sup> Copyright 2014, Wiley-VCH. c) Preparation of the nitrogen-doped graphene-aligned carbon nanotube hybrid materials. Reproduced with permission.<sup>[133]</sup> Copyright 2014, Wiley-VCH.

nanotube hybrid materials were prepared through a template-assisted chemical vapor deposition (CVD) process.<sup>[131]</sup> The protruding carbon nanotubes covalently anchored on the graphene sheets inhibited the stacking of graphene and entanglement of carbon nanotubes, providing compartments between graphene sheets and carbon nanotubes sufficing for sulfur impregnation. The stereo  $sp^2$ -hybridized carbon scaffolds were endowed with an extraordinary conductivity,  $3130 \text{ S cm}^{-1}$  as reported, which enabled the battery to cycle at a high current rate of 5 C without conducting additives. A capacity of  $650 \text{ mA h g}^{-1}$  was retained after 100 cycles with a Coulombic efficiency over 90%. Furthermore, in order to increase the sulfur content, activated pyrolytic carbon was introduced in the conductive  $sp^2$ -hybridized carbon scaffolds (Figure 8b).<sup>[132]</sup> In this hybrid material, seamless-linked graphene–carbon nanotube scaffolds provided efficient pathways for electron transport, while the introduced porous

carbon afforded interconnected micro-/mesopores as electrochemical reservoirs. As a result, 77 wt% of sulfur formed the composite in the hybrid material. It should be mentioned that the electrode is immune from conducting additives, benefited from the conductive graphene/carbon nanotube scaffolds. Therefore, the sulfur content in electrode was 69%, promising a high energy density. The authors declared that the gravimetric energy density of the packaged cell was expected to be  $400 \text{ W h kg}^{-1}$  at a packaged power density of  $10\,000 \text{ W kg}^{-1}$ , approaching the level of engine driven systems. As discussed previously, doping heteroatoms, like nitrogen, in carbon materials will improve the electrochemical performance and catalytic activity.<sup>[112]</sup> Accordingly, N-doped aligned carbon nanotube/graphene hybrid materials were created as scaffolds for sulfur, as illustrated in Figure 7c.<sup>[133]</sup> The doped nitrogen atoms improved the affinity between sulfur and scaffolds, facilitating the deep lithiation of the sulfur. In these hybrid materials, graphene and carbon nanotube are seamlessly linked, which prevents the unwanted aggregation, and is conducive for electrons transport. Therefore, the sulfur is apt to uniformly spread over the large surface area of the hybrid materials. The resultant battery has a decent rate performance that can undergo repeated charge–discharge cycles at a large current.

Apart from the  $sp^2$ -hybridized carbon scaffolds, porous carbon is also chemically constructed on graphene sheets to form a sandwich-type hybrid carbon nanosheets with abundant accessible micropores and mesopores.<sup>[134]</sup> The hybrid material has a large surface area up to  $1558 \text{ m}^2 \text{ g}^{-1}$  and delivered a capacity of  $860 \text{ mA h g}^{-1}$  at 1 C after 100 cycles.

## 2.5. Methods for Composition

In the above sections, we have discussed sulfur cathodes composited with various materials spanning from inorganic particles to hybrid architectures. Here, we will end the story by a summary of different compositing methods involved in preparing the sulfur cathodes. Reviewing a number of papers reporting high-performance sulfur cathodes, there are six methods primarily applied that are listed in **Table 1**.

Initially, the ball-milling method was usually adopted to mix the sulfur with inorganic particles, but its production where sulfur and particles are weakly bound does not benefit for a good performance. On this account, the ball milling is less concerned afterward especially when porous carbon is

Table 1. Summary of representative composition methods for sulfur cathodes.

Methods	Temp.	Sulfur size	Affinity	Application	Ref
Milling	r.t. <sup>a)</sup>	μm	weak	inorganic, carbon particles	[56]
Melt-diffusion	150–160 °C	ca. 10 nm to μm	strong	General	[37,58,94]
Vapor infusion	300–500 °C	ca. 10 nm to μm	strong	hollow particles	[53,61,62]
Chemical deposition	0 °C–r.t.	ca. 10 <sup>2</sup> nm to μm	moderate	2D, 3D materials	[106,121]
Precipitation	r.t.	ca. 10 <sup>2</sup> nm to μm	moderate	particles, 1D materials	[71,84]
in situ composition	variable <sup>b)</sup>	ca. 10 nm to μm	strong	polymer, inorganic particles	[28,55]

<sup>a)</sup>In general, room temperature (r.t.) refers to 25 °C; <sup>b)</sup>The temperature for in situ composition depends on the synthesis requirements of different materials.

used as sulfur host. Recently, however, this method has been rejuvenated when expanded to prepare graphene–sulfur composite and lithium sulfide cathodes.<sup>[114,135,136]</sup>

The melt-diffusion strategy is the most widely applied method to prepare sulfur cathode, which takes advantage of the unique viscosity-temperature behavior of sulfur melt. When the solid  $\alpha$ -sulfur is heated, the viscosity of sulfur melt decreases slowly until it sharply increases around 160 °C, where the octa-sulfur ring opens and polymerizes. To this regard, the pristine sulfur is normally pre-milled with host materials and then hermetically heated at 150–160 °C. The sulfur melt will infiltrate into the host materials and fill the porous structures driven by capillary forces. Afterward, it solidifies and shrinks to form sulfur crystals that intimately contact with the conducting matrix. The complete filling of sulfur is commonly confirmed by Brunauer–Emmett–Teller (BET) measurements, which indicate a dramatic decrease of pore volumes. The melt-diffusion strategy is popularized in the wake of the success of porous materials as sulfur reservoir and is adaptable for a large variety of materials with pore volume spanning from nanometers to micrometers. Then the ball-milling method used in early research is gradually abandoned. Similarly, the vapor infusion method uses the phase transition for composition at a higher temperature in the range of 300–500 °C. Sulfur in the gas phase has more freedom than melt sulfur to permeate through porous shells, so vapor infusion is beneficial for compositing sulfur with hollow particles.<sup>[53,61,62]</sup> In some cases, we can realize a molecular level mixing through this method, but, compared with the melt-diffusion strategy, the vapor-infusion method brings about more safety considerations, which are unfavorable for large-scale production.

Compositing by chemical deposition and solution precipitation is usually carried out at ambient condition. Chemical deposition involves the disproportionation of thiosulfate. The reaction can be expressed as:  $S_2O_3^{2-} + 2H^+ \rightarrow S \downarrow + SO_2 \uparrow + H_2O$ . The sulfur precipitates accompanying the emission of sulfur dioxide. Typically, sodium thiosulfate and hydrochloric acid or sulfuric acid are preferred as reagents. The reaction is carried out in moderate conditions and through a simple procedure in which acid is slowly added dropwise into thiosulfate solution under vigorous stirring, whereupon sulfur suspensions are produced. In many cases, surfactant polymers like poly(vinylpyrrolidone) (PVP) are added to prevent aggregation and form small and uniform sulfur particles.<sup>[54,104,110]</sup> The combination of sulfur and a host

material usually takes place in solution under stirring. Hence, this method is particularly suitable for compositing sulfur with 2D materials like graphene because its basal plane is favorable for nucleation and attaching. Solution precipitation is not as widely-used among various materials as melt-diffusion strategy and chemical deposition. It is a simple physical process that sulfur recrystallizes and separates out when the solvent evaporates. Carbon disulfide with a large solubility of sulfur is often selected as the solvent. However, solution precipitation can hardly produce small and uniform sulfur particles so assistant process, like ultrasonication, is always required.<sup>[71,84]</sup>

The in situ composition is a bottom-up process that is commonly-used in constructing a core–shell structure. In a general procedure, sulfur particles are first mixed with monomers that are prone to absorb on the surface of sulfur particles. Then, the monomers polymerize to form a polymer shell that encases the sulfur particles.<sup>[51,52,55]</sup> The bottom-up process can produce composite particles with size ranging from several hundred nanometers to micrometers, which is determined by the initial sulfur particles. It is often the case that the above-mentioned methods are used in combination. For example, when fill sulfur in complex architectures like Figure 2b, solution precipitation is first used to pre-disperse before heating to 155 °C.<sup>[29]</sup> Moreover, uniform sulfur particles are usually prepared through chemical deposition or solution precipitation before in situ synthesizing a polymer or inorganic shell outside.<sup>[28]</sup>

### 3. Anodes

Compared with the sulfur cathode that has been diversified in a number of papers, the anode of the lithium–sulfur battery seems to have been abandoned. The majority of the lithium–sulfur batteries discussed to date employ metallic lithium as the anode. Although the lithium anode has a large theoretical capacity of 3860 mA h g<sup>-1</sup>, its drawbacks, especially regarding safety vulnerabilities, have restricted lithium–sulfur battery applications. The lithium anode is apt to form dendrites arising from the unstable solid electrolyte interphase (SEI), which may cause a short-circuit once piercing the separator. In addition, the fresh lithium exposed will trigger an unwanted parasitic reaction with polysulfides, leading to shuttle effects that decrease the Coulombic efficiency. As flexible and wearable devices are burgeoning, the

lithium anode, unfortunately, makes the battery unadaptable for deformation and incompatible for flexibility.<sup>[119,137]</sup> To this end, a reliable lithium-free anode, such as that which has materialized in lithium-ion batteries, is badly needed and is highly desired for lithium–sulfur batteries.<sup>[2,3]</sup>

Currently, several lithium-free anodes have been reported to be compatible with the sulfur cathodes including tin-based anode, silicon anode and carbon anode.<sup>[138–140]</sup> Once the metallic lithium is removed, the lithium ions can be stored either in cathode or anode. Provided that the cathode is employed as lithium source, a lithiated sulfur compound like lithium sulfide ( $\text{Li}_2\text{S}$ ), should be used as cathode material that concurrently served as sulfur and lithium reservoir.<sup>[135,136,141–146]</sup> As a result, the produced battery is in “discharged” state. The lithium sulfide has a theoretical capacity of  $1166 \text{ mA h g}^{-1}$  and is normally considered as electrochemically inactive. Cui and co-workers discovered that a potential barrier (ca. 1 V) was entailed during the initial charge for  $\text{Li}_2\text{S}$  which was derived from the phase nucleation of polysulfides.<sup>[143]</sup> For another case where lithium is stored in the anode, the anode material should be lithiated first, whereupon the lithium ions will remove from the anode and migrate to the cathode when discharged.<sup>[140,147–149]</sup>

### 3.1. Tin Anodes

In 2010, Hassoun and Scrosati reported a metallic-lithium-free lithium–sulfur battery with a  $\text{Li}_2\text{S}$ –C composite cathode and a Sn–C composite anode.<sup>[138]</sup> Tin has been previously studied as the anode material in lithium-ion batteries. Metallic tin can electrochemically react with lithium to form lithium alloy that contains 4.4 lithium atoms per tin atom, providing a large specific capacity of  $994 \text{ mA h g}^{-1}$ .<sup>[150]</sup> However, like other lithium metal alloys, Li–Sn alloy is annoyed by the significant volume change in the cycle of lithiation and delithiation. On this account, a carbon matrix is introduced to buffer the effect of volume expansion. The Sn–C composite was paired with  $\text{Li}_2\text{S}$ –C composite cathode across a polymer gel electrolyte. Although the voltage profile displayed an indiscernible plateau and showed a large polarization, the full battery performed normally at 0.05 C giving a capacity approaching  $1200 \text{ mA h g}^{-1}$ , which was retained at over  $800 \text{ mA h g}^{-1}$  after 35 cycles. At higher rate of 0.2 C, the battery operated steadily over 90 cycles, indicating the feasibility of the Sn–C anode as the surrogate of metallic lithium.

### 3.2. Silicon Anodes

Silicon is a promising anode material for lithium-ion batteries, with a theoretical capacity of  $4200 \text{ mA h g}^{-1}$ . The voltage plateau in discharge profile is around 0.3 V vs  $\text{Li/Li}^+$ .<sup>[151]</sup> The large capacity and low discharge potential can promise a high energy density of the full cell. However, the silicon anode is annoyed by some tricky issues including the volume expansion (ca. 400%) and unstable solid electrolyte interphase

film, which lead to the pulverization of the electrode, severe capacity fading, and low Coulombic efficiency. Moreover, the inferior electrical conductivity and ionic mobility of silicon also cause large polarization and undermine the rate performances of the battery.<sup>[152,153]</sup> These problems loom large when paired with a sulfur cathode to fabricate a full cell.

As previously mentioned, replacing metallic lithium in the anode necessitates a lithiated cathode or a lithiated anode to provide lithium ions. Cui and co-workers made the first attempt at employing silicon nanowires as the anode while compositing  $\text{Li}_2\text{S}$  with CMK-3 as the cathode.<sup>[144]</sup> The discharge profile displayed a distinct plateau at 1.7 V since the discharge potential for a silicon anode is ca. 0.4 V vs  $\text{Li/Li}^+$ . The full cell delivered an initial discharge capacity of  $482 \text{ mA h g}^{-1}$  and an energy density of  $630 \text{ W h kg}^{-1}$  considering the active materials, yet the capacity suffered a 50% degradation over 20 cycles, implying the full cell was reluctant to undergo a long time operation. Parasitic reactions occurring in the full cell were ascribable since they irreversibly consumed lithium ions that could not be replenished by the limited lithium storage in electrodes. Another strategy in which the silicon is prelithiated as the anode seems more popular because it can employ the sulfur cathode, which is mature in technique and focuses on optimizing the silicon anode. Aurbach and co-workers reported a lithium–sulfur full cell employing lithiated amorphous silicon film as anode and sulfur/carbon black composite as cathode.<sup>[148]</sup> The full cell can deliver a capacity of  $384 \text{ mA h g}^{-1}$  after decaying from  $600 \text{ mA h g}^{-1}$  over 60 cycles. The enhanced longevity and stability as well as the high Coulombic efficiency (>90%) suggested the feasibility of the lithiated silicon as anode. The performance was further improved by introducing an ionic liquid electrolyte, as reported by Guo and co-workers.<sup>[149]</sup> Moreover, the sulfur cathode was replaced by a composite of small sulfur molecules and carbon nanomaterials.<sup>[73]</sup> As a result, the full cell delivered a reversible capacity of  $670 \text{ mA h g}^{-1}$  after 50 cycles with Coulombic efficiency nearing ca. 100%. Hence, the safety issue of the battery was significantly alleviated by replacing the metallic lithium and liquid electrolyte. It was acclaimed as great progress that the concept of the lithium–sulfur full cell has been successfully realized, but it is also alarming that the cyclic stability of the available full cell is rather low, which cannot afford practical applications.

Kaskel and co-workers took a great leap forward producing a balanced and stable lithium–sulfur full cell that can sustain 1000 reversible cycles.<sup>[147]</sup> They sputtered amorphous silicon on a carbon cloth rendering a flexible anode. In their efforts toward ultra-long cycles, producing a reliable and stable silicon anode played a critical part. They adopted a delicate strategy that partially lithiates the anode inspiring by the fact that the cyclic stability of silicon anode can be significantly enhanced by limiting the degree of lithiation.<sup>[154]</sup> As a result, they obtained a stable silicon anode that can undergo over 300 cycles without obvious degradation, which is of great importance for a high-performance full cell. After pairing with a cathode prepared from hollow carbon spheres and sulfur, the full cell was obtained and displayed a high capacity and stability over 1000 reversible cycles.

### 3.3. Carbon Anodes

Carbon materials, especially graphite with discrete graphene layers, are widely used as host materials in conventional lithium-ion batteries. The application of carbon materials, including graphite and hard carbons, is also reported. Wang and co-workers employed commercial graphite to pair with a  $\text{Li}_2\text{S}$ /mesoporous carbon composite cathode.<sup>[155]</sup> The full cell gave a discharge voltage potential around 1.6 V and retained its capacity over  $600 \text{ mA h g}^{-1}$  after 150 cycles. It should be noted that the full cell used the conventional carbonate electrolyte (ethylene carbonate/diethyl carbonate). In lithium-ion batteries, the graphite anode is apt to failure due to the co-intercalation of solvent molecules between the graphene layers upon lithiation, which will exfoliate the graphite and damage the layered structure. In carbonate electrolyte like ethylene carbonate, the electrode surface will form a passivation film that protects the electrode from failure.<sup>[156–158]</sup> Thus, the graphite anode prefers a carbonate electrolyte, which, nevertheless, is incompatible in lithium–sulfur batteries. In this case, the  $\text{Li}_2\text{S}$ –mesoporous carbon composite cathode is delicately designed to accommodate the carbonate electrolyte. However, most available sulfur cathodes struggle to operate normally in a carbonate electrolyte. That's why graphite is rarely reported as the anode in lithium–sulfur batteries. Kaskel and co-workers reported another carbon-based anode coating, hard carbon, on carbon-fiber networks. The all-carbon anode was lithiated versus metallic lithium before paring with sulfur cathode. The full cell cycled 550 cycles with a capacity of  $753 \text{ mA h g}^{-1}$ .<sup>[147]</sup>

### 3.4. Hybrid Anodes

Apart from the safety issue, the reactive lithium is also attributed to the battery degradation. The electrochemical corrosion of lithium continuously refresh the surface which favors the reaction with electrolyte and polysulfides to form unstable solid electrolyte interphase (SEI). Therefore, the Coulombic efficiency is decreased and the electrolyte is apt to get depleted. In light of the lithium storage capability of graphite and small volume expansion (<10%) when lithiated, Liu et al. proposed a new hybrid anode where lithiated graphite was placed in front and electrically connected with lithium metal, as displayed in **Figure 9**.<sup>[159]</sup> The short circuit between the lithiated graphite and lithium metal made the graphite always be replenished with lithium ions. The lithiated graphite served as a lithium “pump” that provided lithium ions on demand and were supplied by lithium metal. The introduction of graphite before the lithium metal reduced its contact between lithium–sulfur compounds; thus, parasitic reactions were suppressed, improving the cyclic performance. The hybrid anode does not exclude metallic lithium though, it benefits from the modification and mitigates the intrinsic problems. As metallic lithium plagues all the batteries that use it as anodes, any improvements in lithium anodes derived from other lithium batteries can be expanded to lithium–sulfur batteries.<sup>[160,161]</sup> For example, Cui and co-workers presented a stabilized lithium metal anode coated with a

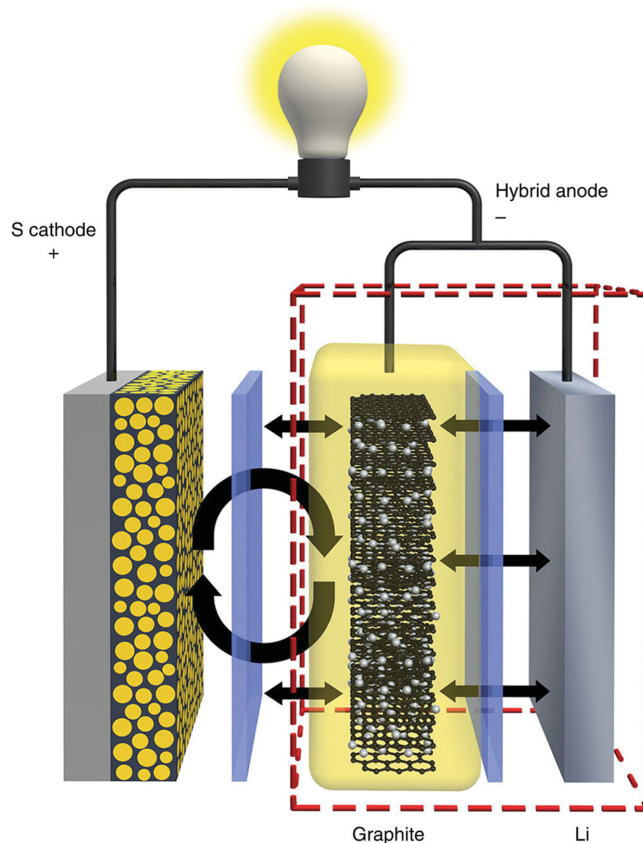


**Figure 9.** Schematic illustration to the hybrid anode design to manipulate the surface reactions in the lithium–sulfur battery. Reproduced with permission.<sup>[159]</sup> Copyright 2014, Nature Publishing Group.

monolayer of interconnected amorphous hollow carbon nanospheres on which formed a stable solid-state electrolyte interphase.<sup>[160]</sup> It is always helpful to expand the attention to lithium-ion batteries in dealing with the anode dilemma in lithium–sulfur batteries.

### 3.5. Lithium Alloy Anodes

Another promising anode instead of metallic lithium is lithium alloys like lithium–boron alloy ( $\text{Li}_7\text{B}_6$ ).<sup>[162,163]</sup> Zhang and co-workers found that the 3D  $\text{Li}_7\text{B}_6$  nanostructure enlarged the specific area and then suppressed the dendrite growth by reducing the current density. Moreover, the nanostructure provided adequate space to stabilize the concentration of Li ions by affecting the lithium re-deposition, leading to a stable interfacial behavior. The lithium–boron alloy anode exhibited remarkable stability and afforded running for 2000 cycles with Coulombic efficiency above 90%, in stark contrast to the lithium plate anode that suffocated at last.<sup>[162]</sup>

The modified lithium anode and the lithium alloy anode can, to some extent, alleviate the intrinsic problems of metallic lithium, but their safety vulnerabilities are not thoroughly removed. The suppressed lithium dendrite and enhanced stability are not sufficient to overcome the constraints imposed by metallic lithium, including the high costs, humidity sensitivity, and incompatibility with applications

pertaining to flexible devices. In this regard, developing a lithium-free anode to replace metallic lithium in lithium-sulfur batteries is still necessary and contributory for its permeation into market.

#### 4. Flexible Electrodes

The staggering increase of wearable devices has increased interest in flexible batteries. It is often the case that attempts to make the device flexible and conformable to wearability spring up in the wake of its emergence. Currently lithium-ion batteries have been successfully transformed into flexible configuration and fiber shape, which inspires the fabrication of flexible lithium-sulfur batteries.<sup>[2,3,164–166]</sup> As the flexible battery strongly relies on the flexible electrodes, things become tricky when encountering metallic lithium anode in lithium-sulfur batteries, which highlights the importance and necessity of a lithium-free anode. In this regard, the flexible lithium-sulfur battery is not available at present but several works have blazed the trail and started with the preparation of flexible cathode. Aurbach and colleagues developed a binder-free sulfur cathode using activated carbon fiber cloth as sulfur host and conducting substrate.<sup>[81]</sup> Cheng and co-workers impregnated sulfur into the template-synthesized carbon nanotube membranes to make a freestanding sulfur cathode.<sup>[82]</sup> It is concluded that a highly conducting, binder-free and self-standing sulfur cathode is a prerequisite to a flexible battery. 1D carbon materials, like carbon nanotubes and carbon nanofibers, therefore, are widely appreciated as scaffolds since their 1D configuration favors electron transport as well as interconnected framework.<sup>[167–170]</sup> The electrochemical performance of the flexible sulfur cathode is less affected by the absence of binder and conducting diluents. For example, an initial capacity of 995 mA h g<sup>-1</sup> was obtained at 0.05 C which retained by 70% after 150 cycles.<sup>[168]</sup> Unlike other flexible devices, for which the performance has been traced during the process of repeated deformation, however, the flexibility as well as the endurance and sustainability of sulfur cathodes have rarely been investigated, which makes them less conformable to the concept of flexibility. On the other hand, making the lithium anode flexible sounds unfeasible, but it is rational to transform a lithium-free anode toward flexibility. As described previously, Kaskel and co-workers prepared a flexible anode by sputtering the amorphous silicon onto a commercial carbon non-woven, which exhibited decent ability in lithium uptake and delivery.<sup>[147]</sup> Fabricating a flexible lithium-sulfur battery is a formidable challenge, and strategies that proved feasible in flexible lithium-ion batteries can be learned and tried.

#### 5. Challenges and Perspectives

First proposed half a century ago, the lithium-sulfur battery, which is theoretically endowed with high capacity and energy density, has attracted broad interest as scientists and engineers seek approaches to extend the driving range of electric vehicles, regarding it as a competitive candidate for

on-board power systems. However, the development of the lithium-sulfur battery has been bogged down for a couple of years, since its gifted performances suffer a rapid decay over repeated charge-discharge cycles. The battery degradation arises from the unique electrochemical behavior involving two phase-transition reactions. The sulfur dissolution and redistribution leads to irreversible loss of capacity and lithium-sulfur compounds shuttling and reacting with the lithium anode renders a low Coulombic efficiency. Fortunately however, in the wake of the success that Nazar and co-workers had confining the sulfur within the nanochannels of mesoporous carbon to suppress the leakage of polysulfides, scientists are finding ways to enhance the cyclic stability by upgrading the electrode materials and creating novel structures.<sup>[58]</sup> A large variety of sulfur composite cathodes are derived in the following wave of exploitation, which significantly prolongs the charge-discharge cycles. Benefitting from the delicate design of electrodes and an effective strategy, the lithium-sulfur can survive more than 1000 cycles, on a par with lithium-ion batteries (Table 2). In the study of lithium-sulfur batteries, the cyclic number is regarded as a critical index that motivates researchers to spare no efforts to prolong its duration under repeated draining and recharging. At present, the latest lithium-sulfur battery can run more than 2000 cycles.<sup>[112]</sup> However, before acclaiming the longest cycle life as the triumph of a battery, it is worth carefully considering the question: is longer really better?

Probably not. The recent success of cyclic stability may have obscured the original motivation of research – the high energy density. In applications such as military drones, electric vehicles, and portable devices where the lithium-ion battery cannot suffice, the energy density of a candidate battery is probably the priority in consideration. The energy density is closely related to the sulfur content in the cathode. A sketchy comparison between lithium-sulfur batteries and lithium-ion batteries suggests that the sulfur content in the cathode should be at least higher than 50 wt% to retain its superiority in gravimetric energy density over advanced lithium-ion batteries.<sup>[14]</sup> In some cases, nevertheless, the high utilization of sulfur and improved cyclic performance is achieved sacrificing the sulfur loading (30–50 wt%). Figure 10a depicts the relation between the energy density and the sulfur content based on the cathode. The energy density of advanced lithium-ion batteries is based on  $x\text{Li}_2\text{MnO}_3-y\text{LiMO}_2$  cathode which has a theoretical capacity of 250–320 mA h g<sup>-1</sup> and output voltage of 3.5 V. Obviously, many reported lithium-sulfur batteries did not show their intrinsic salient superiority since the delivered energy densities were on par with the advanced lithium-ion batteries. After hundreds of charge-discharge cycles, most of the studied lithium-sulfur batteries degraded beneath the level of their rivals. In the authors' perspective, researchers should shift their focuses to enhancing the energy density of the battery and pay more attention to the cyclic stability rather than a large cyclic number. In most sulfur cathodes, the sulfur content is less than 70 wt% because the additives like binder and conducting agent will account for 10–20% in weight. Increasing the sulfur loading in conducting matrix (>80%) or creating the conducting self-standing cathode which is immune from additives can

Table 2. Summary of representative lithium–sulfur batteries.

Description	Initial capacity [mA h g <sup>-1</sup> ]	Rate [C]	Cycle number	Retained capacity [mA h g <sup>-1</sup> ]	Capacity retention	Sulfur content <sup>a)</sup>	Ref.
CTAB-modified sulfur and graphene oxide composite cathode; ionic liquid electrolyte	1440	0.05	1000	846	58.8%	56%	[111]
Sulfur–graphene oxide core–shell particles	900	0.6	1000	800	88.9%	40%	[104]
Sulfur–nitrogen-doped graphene	789	2	2000	347	44.0%	60%	[112]
Sulfur–graphene wrapping carbon nanofibers composite cathode	745	1	1500	273	36.6%	33%	[129]
Sulfur–yolk shell TiO <sub>2</sub> architecture	1030	0.5	1000	690	67.0%	53%	[28]
Polymer-encapsulated hollow sulfur nanospheres	990	0.5	1000	535	54.0%	49%	[54]
Encapsulating monoclinic sulfur within carbon nanotubes	1138	5 <sup>b)</sup>	1000	863	75.8%	81%	[175]
Silicon–carbon anode & sulfur–hollow carbon cathode	ca. 1050 <sup>c)</sup>	0.5	1390	ca. 400 <sup>c)</sup>	38.1%	53%	[147]
Matching the sulfur/electrolyte loading; sulfur–carbon nanotube cathode	1053	1	1000	537	51.0%	–	[176]
Sulfur–unstacked double-layer templated graphene	1034	5	1000	530	51.3%	57%	[116]
Sulfur–hollow polyaniline sphere	ca. 1200 <sup>c)</sup>	0.5	1000	602	50.2%	50%	[53]

<sup>a)</sup>The sulfur content is based on the entire cathode; <sup>b)</sup>The battery was recharged at 2 C; <sup>c)</sup>The capacity is estimated from the figure. The authors did not provide the specific number in the paper.

be effective approaches to raise the sulfur content in the cathode. Moreover, for a commercially viable candidate for future batteries, the performance stability over charges is more important than its advertised advancements. From Figure 10b we can conclude that high capacity retention (>80%) after long cycles (>500) was rarely reported, which indicates the direction of improvement. Apart from refining the sulfur cathodes, strategies like manipulating the charge process, introducing the functional interlayers and modifying the electrolyte are very helpful to keep the performances insusceptible for repeated recharges.<sup>[12,14,159,171]</sup> It should be noted that the performances of a battery are multifacetedly affected and it is often the case that in many communications, some critical details like sulfur content, the dosage of electrolyte and current rate, are obscured in order to highlight one or two remarkable indexes. Thus, it is necessary to build up standardized measurements to gauge any modification to lithium–sulfur batteries that is claimed as improvement.

Another challenge at the forefront of lithium–sulfur battery technology is the safety issue. As we discussed before, most lithium–sulfur batteries have metallic lithium as their anodes. The lithium anode, indeed, is one of the safety vulnerabilities of lithium–sulfur batteries, as the lithium dendrite formed on the surface of the anode is likely to pierce the separator and cause a short circuit. Replacing the metallic lithium and finding a successor, like graphite in lithium-ion batteries, to fabricate a metallic-lithium-free full battery is an effective strategy to solve this problem. However, finding an eligible anode that is comparable in capacity and compatible with the electrolyte is not easy, and coupling the anode with a sulfur cathode requires more attempts to accumulate empirical details in matching the capacities. Nevertheless, this formidable challenge is in stark contrast to

the stagnant study. To the best of our knowledge, amongst published papers relating lithium–sulfur batteries, those pertaining to metallic-lithium-free anodes merely account for less than 10%, while 67% of papers are concerned with the sulfur cathode. As the intensive investigation in sulfur cathodes progresses, the obstacle once hindering the development of lithium–sulfur batteries is gradually wiped out. The lithium anode has become the major stumbling block that obstructs its ubiquity. More efforts should be devoted in this area. Furthermore, coupling with a metallic-lithium-free anode will inevitably reduce the output voltage, which in reverse, will boost the study of sulfur cathodes to squeeze more capacity, and retain its superiority in energy density over lithium-ion batteries. The electrolyte is the other safety vulnerability. Conventional electrolytes in lithium–sulfur batteries are toxic and flammable, which causes serious hazards should they leak out. A non-flammable electrolyte, such as solid-state electrolytes or ionic liquids can eliminate this issue.<sup>[172,173]</sup> Flame-retardant additives in electrolytes have also been proved feasible.<sup>[174]</sup>

On the list of candidates for future batteries, the lithium–sulfur battery is edging ahead of its competitors, like lithium–air batteries and sodium-ion batteries, which are still wrestling with problems in the lab, as a promising successor to lithium-ion batteries. The major problem of battery degradation that once impeded the progress of application is significantly alleviated by using a sulfur cathode. The safety vulnerabilities of metallic lithium and the liquid electrolyte are remedied by the attempts at fabricating metallic-lithium-free batteries and modifying flame-retardant electrolytes. Despite steps toward applications still encountering many challenges, the recent progress still paints an encouraging picture of a revolution in rechargeable batteries.

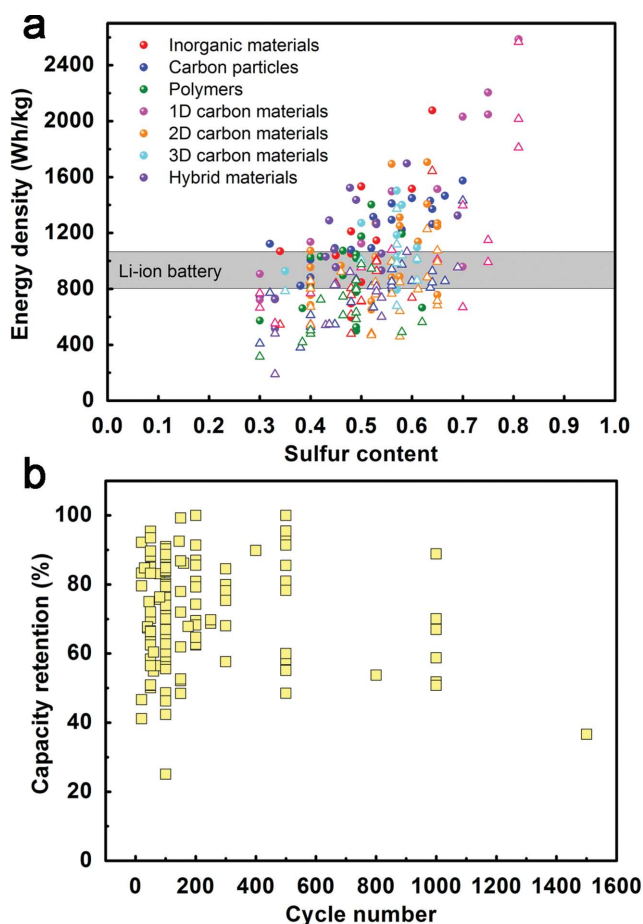


Figure 10. Review of the reported results. a) The plot of energy density (based on cathode) and sulfur content of the cathode before (circles  $\circ$ ) and after (triangles  $\Delta$ ) running for cycles. b) The capacity retention of the reported lithium-sulfur batteries after running for cycles.

## Acknowledgements

This work was supported by MOST (2011CB932503), NSFC (21225417), STCSM (12nm0503200), the Fok Ying Tong Education Foundation, the Program for Special Appointments of Professors at Shanghai Institutions of Higher Learning, and the Program for Outstanding Young Scholars from the Organization Department of the CPC Central Committee.

[1] J. Ren, L. Li, C. Chen, X. Chen, Z. Cai, L. Qiu, Y. Wang, X. Zhu, H. Peng, *Adv. Mater.* **2013**, *25*, 1155–1159.  
 [2] J. Ren, Y. Zhang, W. Bai, X. Chen, Z. Zhang, X. Fang, W. Weng, Y. Wang, H. Peng, *Angew. Chem. Int. Ed.* **2014**, *53*, 7864–7869.  
 [3] Y. Zhang, W. Bai, J. Ren, W. Weng, H. Lin, Z. Zhang, H. Peng, *J. Mater. Chem. A* **2014**, *2*, 11054–11059.  
 [4] Z. Zhang, Z. Yang, Z. Wu, G. Guan, S. Pan, Y. Zhang, H. Li, J. Deng, B. Sun, H. Peng, *Adv. Energy Mater.* **2014**, DOI: 10.1002/aenm.201301750.  
 [5] S. Pan, Z. Yang, P. Chen, J. Deng, H. Li, H. Peng, *Angew. Chem. Int. Ed.* **2014**, *126*, 6224–6228.

[6] H. Danuta, U. Juliusz, *US Patent 3,043,896*, **1962**.  
 [7] C. Barchasz, J. C. Leprêtre, F. Alloin, S. Patoux, *J. Power Sources* **2012**, *199*, 322–330.  
 [8] J. Zheng, M. Gu, C. Wang, P. Zuo, P. K. Koech, J. Zhang, J. Liu, J. Xiao, *J. Electrochem. Soc.* **2013**, *160*, A1992–A1996.  
 [9] S. S. Zhang, *Electrochem. Commun.* **2013**, *31*, 10–12.  
 [10] L. Yuan, X. Qiu, L. Chen, W. Zhu, *J. Power Sources* **2009**, *189*, 127–132.  
 [11] S. Walus, C. Barchasz, J.-F. Colin, J.-F. Martin, E. Elkaim, J.-C. Leprêtre, F. Alloin, *Chem. Commun.* **2013**, *49*, 7899–7901.  
 [12] Y. Su, Y. Fu, T. Cochell, A. Manthiram, *Nat. Commun.* **2013**, *4*, 2985–2992.  
 [13] P. G. Bruce, S. A. Freunberger, L. J. Hardwick, J. M. Tarascon, *Nat. Mater.* **2012**, *11*, 19–29.  
 [14] L. Suo, Y. Hu, H. Li, M. Armand, L. Chen, *Nat. Commun.* **2013**, *4*, 1481–1489.  
 [15] E. SungáShin, S. HyoungáOh, W. IláCho, *Chem. Commun.* **2013**, *49*, 2004–2006.  
 [16] S. S. Zhang, *Energies* **2012**, *5*, 5190–5197.  
 [17] J. Zheng, D. Lv, M. Gu, C. Wang, J. Zhang, J. Liu, J. Xiao, *J. Electrochem. Soc.* **2013**, *160*, A2288–A2292.  
 [18] S. S. Zhang, *Electrochim. Acta* **2012**, *70*, 344–348.  
 [19] D. Aurbach, E. Pollak, R. Elazari, G. Salitra, C. S. Kelley, J. Affinito, *J. Electrochem. Soc.* **2009**, *156*, A694–A702.  
 [20] S. S. Zhang, *J. Electrochem. Soc.* **2012**, *159*, A920–A923.  
 [21] M. S. Song, S. C. Han, H. S. Kim, J. H. Kim, K. T. Kim, Y. M. Kang, H. J. Ahn, S. Dou, J. Y. Lee, *J. Electrochem. Soc.* **2004**, *151*, A791–A795.  
 [22] W. Zheng, X. G. Hu, C. F. Zhang, *Electrochem. Solid-State Lett.* **2006**, *9*, A364–A367.  
 [23] Y. Zhang, X. Wu, H. Feng, L. Wang, A. Zhang, T. Xia, H. Dong, *Int. J. Hydrogen Energy* **2009**, *34*, 1556–1559.  
 [24] Y. J. Choi, B. S. Jung, D. J. Lee, J. H. Jeong, K. W. Kim, H. J. Ahn, K. K. Cho, H. B. Gu, *Phys. Scr.* **2007**, *2007*, 62.  
 [25] K. Dong, S. Wang, H. Zhang, J. Wu, *Mater. Res. Bull.* **2013**, *48*, 2079–2083.  
 [26] B. Ding, L. Shen, G. Xu, P. Nie, X. Zhang, *Electrochim. Acta* **2013**, *107*, 78–84.  
 [27] Q. Li, Z. Zhang, K. Zhang, L. Xu, J. Fang, Y. Lai, J. Li, *J. Solid State Electrochem.* **2013**, *17*, 2959–2965.  
 [28] Z. W. Seh, W. Li, J. J. Cha, G. Zheng, Y. Yang, M. T. McDowell, P. C. Hsu, Y. Cui, *Nat. Commun.* **2013**, *4*, 1331–1336.  
 [29] Z. Liang, G. Zheng, W. Li, Z. W. Seh, H. Yao, K. Yan, D. Kong, Y. Cui, *ACS Nano* **2014**, *8*, 5249–5256.  
 [30] N. Liu, H. Wu, M. T. McDowell, Y. Yao, C. Wang, Y. Cui, *Nano Lett.* **2012**, *12*, 3315–3321.  
 [31] G. de Combarieu, M. Morcrette, F. Millange, N. Guillou, J. Cabana, C. P. Grey, I. Margiolaki, G. Férey, J. M. Tarascon, *Chem. Mater.* **2009**, *21*, 1602–1611.  
 [32] G. Férey, F. Millange, M. Morcrette, C. Serre, M. L. Doublet, J. M. Grenèche, J. M. Tarascon, *Angew. Chem. Int. Ed.* **2007**, *46*, 3259–3263.  
 [33] J. Zhou, R. Li, X. Fan, Y. Chen, R. Han, W. Li, J. Zheng, B. Wang, X. Li, *Energy Environ. Sci.* **2014**, *7*, 2715–2724.  
 [34] R. Demir Cakan, M. Morcrette, F. Nouar, C. Davoisne, T. Devic, D. Gonbeau, R. Dominko, C. Serre, G. Férey, J. M. Tarascon, *J. Am. Chem. Soc.* **2011**, *133*, 16154–16160.  
 [35] W. Bao, Z. Zhang, Y. Qu, C. Zhou, X. Wang, J. Li, *J. Alloys Compd.* **2014**, *582*, 334–340.  
 [36] Z. Zhao, S. Wang, R. Liang, Z. Li, Z. Shi, G. Chen, *J. Mater. Chem. A* **2014**, *2*, 13509–13512.  
 [37] J. Zheng, J. Tian, D. Wu, M. Gu, W. Xu, C. Wang, F. Gao, M. H. Engelhard, J. Zhang, J. Liu, J. Xiao, *Nano Lett.* **2014**, *14*, 2345–2352.  
 [38] Q. Pang, D. Kundu, M. Cuisinier, L. F. Nazar, *Nat. Commun.* **2014**, *5*, 4759.  
 [39] X. Tao, J. Wang, Z. Ying, Q. Cai, G. Zheng, Y. Gan, H. Huang, Y. Xia, C. Liang, W. Zhang, Y. Cui, *Nano Lett.* **2014**, *14*, 5288–5294.

- [40] K. S. Park, S. B. Schougaard, J. B. Goodenough, *Adv. Mater.* **2007**, *19*, 848–851.
- [41] P. Novák, K. Müller, K. Santhanam, O. Haas, *Chem. Rev.* **1997**, *97*, 207–282.
- [42] X. Chen, H. Lin, P. Chen, G. Guan, J. Deng, H. Peng, *Adv. Mater.* **2014**, *26*, 4444–4449.
- [43] Z. Cai, L. Li, J. Ren, L. Qiu, H. Lin, H. Peng, *J. Mater. Chem. A* **2013**, *1*, 258–261.
- [44] H. Lin, L. Li, J. Ren, Z. Cai, L. Qiu, Z. Yang, H. Peng, *Sci. Rep.* **2013**, *3*, 1353–1358.
- [45] J. Wang, J. Yang, J. Xie, N. Xu, *Adv. Mater.* **2002**, *14*, 963–965.
- [46] J. Wang, J. Yang, C. Wan, K. Du, J. Xie, N. Xu, *Adv. Funct. Mater.* **2003**, *13*, 487–492.
- [47] J. Wang, J. Chen, K. Konstantinov, L. Zhao, S. H. Ng, G. Wang, Z. Guo, H. K. Liu, *Electrochim. Acta* **2006**, *51*, 4634–4638.
- [48] X. Liang, Y. Liu, Z. Wen, L. Huang, X. Wang, H. Zhang, *J. Power Sources* **2011**, *196*, 6951–6955.
- [49] X. Liang, Z. Wen, Y. Liu, X. Wang, H. Zhang, M. W. Huang, *Solid State Ionics* **2011**, *192*, 347–350.
- [50] Y. Fu, A. Manthiram, *RSC Adv.* **2012**, *2*, 5927–5929.
- [51] F. Wu, J. Chen, R. Chen, S. Wu, L. Li, S. Chen, T. Zhao, *J. Phys. Chem. C* **2011**, *115*, 6057–6063.
- [52] H. Chen, W. Dong, J. Ge, C. Wang, X. Wu, W. Lu, L. Chen, *Sci. Rep.* **2013**, *3*.
- [53] G. Ma, Z. Wen, J. Jin, Y. Lu, X. Wu, M. Wu, C. Chen, *J. Mater. Chem. A* **2014**, *2*, 10350–10354.
- [54] W. Li, G. Zheng, Y. Yang, Z. W. Seh, N. Liu, Y. Cui, *Proc. Natl. Acad. Sci. USA* **2013**, *110*, 7148–7153.
- [55] W. Zhou, Y. Yu, H. Chen, F. J. DiSalvo, H. D. Abruna, *J. Am. Chem. Soc.* **2013**, *135*, 16736–16743.
- [56] B. H. Jeon, J. H. Yeon, K. M. Kim, I. J. Chung, *J. Power Sources* **2002**, *109*, 89–97.
- [57] J. Wang, S. Y. Chew, Z. W. Zhao, S. Ashraf, D. Wexler, J. Chen, S. H. Ng, S. L. Chou, H. K. Liu, *Carbon* **2008**, *46*, 229–235.
- [58] X. Ji, K. T. Lee, L. F. Nazar, *Nat. Mater.* **2009**, *8*, 500–506.
- [59] B. Zhang, X. Qin, G. R. Li, X. P. Gao, *Energy Environ. Sci.* **2010**, *3*, 1531–1537.
- [60] J. Schuster, G. He, B. Mandlmeier, T. Yim, K. T. Lee, T. Bein, L. F. Nazar, *Angew. Chem. Int. Ed.* **2012**, *51*, 3591–3595.
- [61] N. Jayaprakash, J. Shen, S. S. Mogganty, A. Corona, L. A. Archer, *Angew. Chem. Int. Ed.* **2011**, *50*, 5904–5908.
- [62] C. Zhang, H. B. Wu, C. Yuan, Z. Guo, X. W. Lou, *Angew. Chem. Int. Ed.* **2012**, *51*, 9592–9595.
- [63] G. He, S. Evers, X. Liang, M. Cuisinier, A. Garsuch, L. F. Nazar, *ACS Nano* **2013**, *7*, 10920–10930.
- [64] X. Li, Y. Cao, W. Qi, L. V. Saraf, J. Xiao, Z. Nie, J. Mietek, J. Zhang, B. Schwenzer, J. Liu, *J. Mater. Chem.* **2011**, *21*, 16603–16610.
- [65] J. Zheng, M. Gu, M. J. Wagner, K. A. Hays, X. Li, P. Zuo, C. Wang, J. Zhang, J. Liu, J. Xiao, *J. Electrochem. Soc.* **2013**, *160*, A1624–A1628.
- [66] X. Y. Zhao, J. P. Tu, Y. Lu, J. B. Cai, Y. J. Zhang, X. L. Wang, C. D. Gu, *Electrochim. Acta* **2013**, *113*, 256–262.
- [67] Y. Yang, G. Yu, J. J. Cha, H. Wu, M. Vosgueritchian, Y. Yao, Z. Bao, Y. Cui, *ACS Nano* **2011**, *5*, 9187–9193.
- [68] X. Zhou, J. Xie, J. Yang, Y. Zou, J. Tang, S. Wang, L. Ma, Q. Liao, *J. Power Sources* **2013**, *243*, 993–1000.
- [69] J. Song, T. Xu, M. L. Gordin, P. Zhu, D. Lv, Y.-B. Jiang, Y. Chen, Y. Duan, D. Wang, *Adv. Funct. Mater.* **2014**, *24*, 1243–1250.
- [70] X. Li, X. Li, M. N. Banis, B. Wang, A. Lushington, X. Cui, R. Li, T. K. Sham, X. A. Sun, *J. Mater. Chem. A* **2014**, *2*, 12866–12872.
- [71] S. Zheng, F. Yi, Z. Li, Y. Zhu, Y. Xu, C. Luo, J. Yang, C. Wang, *Adv. Funct. Mater.* **2014**, *24*, 4156–4163.
- [72] J. L. Wang, J. Yang, J. Y. Xie, N. X. Xu, Y. Li, *Electrochem. Commun.* **2002**, *4*, 499–502.
- [73] S. Xin, L. Gu, N. Zhao, Y. Yin, L. Zhou, Y. Guo, L. Wan, *J. Am. Chem. Soc.* **2012**, *134*, 18510–18513.
- [74] Z. Li, L. Yuan, Z. Yi, Y. Sun, Y. Liu, Y. Jiang, Y. Shen, Y. Xin, Z. Zhang, Y. Huang, *Adv. Energy Mater.* **2014**, DOI: 10.1002/aenm.201301473.
- [75] Z. Li, Y. Jiang, L. Yuan, Z. Yi, C. Wu, Y. Liu, P. Strasser, Y. Huang, *ACS Nano* **2014**, *8*, 9295–9303.
- [76] S. Huang, L. Li, Z. Yang, L. Zhang, H. Saiyin, T. Chen, H. Peng, *Adv. Mater.* **2011**, *23*, 4707–4710.
- [77] H. Lin, W. Weng, J. Ren, L. Qiu, Z. Zhang, P. Chen, X. Chen, J. Deng, Y. Wang, H. Peng, *Adv. Mater.* **2014**, *26*, 1217–1222.
- [78] Z. Yang, T. Chen, R. He, G. Guan, H. Li, L. Qiu, H. Peng, *Adv. Mater.* **2011**, *23*, 5436–5439.
- [79] T. Chen, S. Wang, Z. Yang, Q. Feng, X. Sun, L. Li, Z. S. Wang, H. Peng, *Angew. Chem. Int. Ed.* **2011**, *50*, 1815–1819.
- [80] S. Huang, Z. Yang, L. Zhang, R. He, T. Chen, Z. Cai, Y. Luo, H. Lin, H. Cao, X. Zhu, *J. Mater. Chem.* **2012**, *22*, 16833–16838.
- [81] R. Elazari, G. Salitra, A. Garsuch, A. Panchenko, D. Aurbach, *Adv. Mater.* **2011**, *23*, 5641–5644.
- [82] G. Zhou, D. Wang, F. Li, P. Hou, L. Yin, C. Liu, G. Lu, I. R. Gentle, H. Cheng, *Energy Environ. Sci.* **2012**, *5*, 8901–8906.
- [83] K. Jin, X. Zhou, L. Zhang, X. Xin, G. Wang, Z. Liu, *J. Phys. Chem. C* **2013**, *117*, 21112–21119.
- [84] L. Sun, M. Li, Y. Jiang, W. Kong, K. Jiang, J. Wang, S. Fan, *Nano Lett.* **2014**, *14*, 4044–4049.
- [85] Y. Su, Y. Fu, A. Manthiram, *Phys. Chem. Chem. Phys.* **2012**, *14*, 14495–14499.
- [86] L. Ji, M. Rao, S. Aloni, L. Wang, E. J. Cairns, Y. Zhang, *Energy Environ. Sci.* **2011**, *4*, 5053–5059.
- [87] J. Guo, Y. Xu, C. Wang, *Nano Lett.* **2011**, *11*, 4288–4294.
- [88] G. Zheng, Y. Yang, J. J. Cha, S. S. Hong, Y. Cui, *Nano Lett.* **2011**, *11*, 4462–4467.
- [89] G. Zheng, Q. Zhang, J. J. Cha, Y. Yang, W. Li, Z. W. Seh, Y. Cui, *Nano Lett.* **2013**, *13*, 1265–1270.
- [90] S. Zhang, Q. Zhang, J. Huang, X. Liu, W. Zhu, M. Zhao, W. Qian, F. Wei, *Particle Particle Syst. Charact.* **2013**, *30*, 158–165.
- [91] H. Peng, T. Hou, Q. Zhang, J. Huang, X. Cheng, M. Guo, Z. Yuan, L. He, F. Wei, *Adv. Mater. Interfaces* **2014**, DOI: 10.1002/admi.201400227.
- [92] X. Cheng, J. Huang, Q. Zhang, H. Peng, M. Zhao, F. Wei, *Nano Energy* **2014**, *4*, 65–72.
- [93] Z. Xiao, Z. Yang, H. Nie, Y. Lu, K. Yang, S. Huang, *J. Mater. Chem. A* **2014**, *2*, 8683–8689.
- [94] Y. Zhao, W. Wu, J. Li, Z. Xu, L. Guan, *Adv. Mater.* **2014**, *26*, 5113–5118.
- [95] Y. Zhu, S. Murali, W. Cai, X. Li, J. W. Suk, J. R. Potts, R. S. Ruoff, *Adv. Mater.* **2010**, *22*, 3906–3924.
- [96] Z. Xu, C. Gao, *Acc. Chem. Res.* **2014**, *47*, 1267–1276.
- [97] H. Sun, Z. Xu, C. Gao, *Adv. Mater.* **2013**, *25*, 2554–2560.
- [98] Z. Xu, C. Gao, *Nat. Commun.* **2011**, *2*, 571–579.
- [99] Z. Yang, H. Sun, T. Chen, L. Qiu, Y. Luo, H. Peng, *Angew. Chem. Int. Ed.* **2013**, *52*, 7545–7548.
- [100] X. Fang, Z. Yang, L. Qiu, H. Sun, S. Pan, J. Deng, Y. Luo, H. Peng, *Adv. Mater.* **2014**, *26*, 1694–1698.
- [101] L. Qiu, Q. Wu, Z. Yang, X. Sun, Y. Zhang, H. Peng, *Small* **2014**, DOI: 10.1002/sml.201400703.
- [102] H. Wang, Y. Yang, Y. Liang, J. T. Robinson, Y. Li, A. Jackson, Y. Cui, H. Dai, *Nano Lett.* **2011**, *11*, 2644–2647.
- [103] H. Xu, Y. Deng, Z. Shi, Y. Qian, Y. Meng, G. Chen, *J. Mater. Chem. A* **2013**, *1*, 15142–15149.
- [104] J. Rong, M. Ge, X. Fang, C. Zhou, *Nano Lett.* **2014**, *14*, 473–479.
- [105] L. Ji, M. Rao, H. Zheng, L. Zhang, Y. Li, W. Duan, J. Guo, E. J. Cairns, Y. Zhang, *J. Am. Chem. Soc.* **2011**, *133*, 18522–18525.
- [106] C. Zu, A. Manthiram, *Adv. Energy Mater.* **2013**, *3*, 1008–1012.
- [107] L. Q. Lu, L. J. Lu, Y. Wang, *J. Mater. Chem. A* **2013**, *1*, 9173–9181.
- [108] C. Zhang, W. Lv, W. Zhang, X. Zheng, M. Wu, W. Wei, Y. Tao, Z. Li, Q. Yang, *Adv. Energy Mater.* **2014**, DOI: 10.1002/aenm.201301565.
- [109] L. Wang, D. Wang, F. Zhang, J. Jin, *Nano Lett.* **2013**, *13*, 4206–4211.

- [110] W. Zhou, H. Chen, Y. Yu, D. Wang, Z. Cui, F. J. DiSalvo, H. D. Abruna, *ACS Nano* **2013**, *7*, 8801–8808.
- [111] M. Song, Y. Zhang, E. J. Cairns, *Nano Lett.* **2013**, *13*, 5891–5899.
- [112] Y. Qiu, W. Li, W. Zhao, G. Li, Y. Hou, M. Liu, L. Zhou, F. Ye, H. Li, Z. Wei, S. Yang, W. Duan, Y. Ye, J. Guo, Y. Zhang, *Nano Lett.* **2014**, *14*, 4821–4827.
- [113] B. Ding, C. Yuan, L. Shen, G. Xu, P. Nie, Q. Lai, X. Zhang, *J. Mater. Chem. A* **2013**, *1*, 1096–1101.
- [114] T. Lin, Y. Tang, Y. Wang, H. Bi, Z. Liu, F. Huang, X. Xie, M. Jiang, *Energy Environ. Sci.* **2013**, *6*, 1283–1290.
- [115] X. Yang, L. Zhang, F. Zhang, Y. Huang, Y. Chen, *ACS Nano* **2014**, *8*, 5208–5215.
- [116] M. Zhao, Q. Zhang, J. Huang, G. Tian, J. Nie, H. Peng, F. Wei, *Nat. Commun.* **2014**, *5*, 3410–3410.
- [117] S. Chung, A. Manthiram, *Adv. Mater.* **2014**, *26*, 1360–1365.
- [118] G. Xu, B. Ding, L. Shen, P. Nie, J. Han, X. Zhang, *J. Mater. Chem. A* **2013**, *1*, 4490–4496.
- [119] W. Weng, H. Lin, X. Chen, J. Ren, Z. Zhang, L. Qiu, G. Guan, H. Peng, *J. Mater. Chem. A* **2014**, *2*, 9306–9312.
- [120] L. Wang, Y. Zhao, M. L. Thomas, H. R. Byon, *Adv. Funct. Mater.* **2014**, *24*, 2248–2252.
- [121] S. Chen, X. Huang, H. Liu, B. Sun, W. Yeoh, K. Li, J. Zhang, G. Wang, *Adv. Energy Mater.* **2014**, DOI: 10.1002/aenm.201301761.
- [122] S. Lu, Y. Chen, X. Wu, Z. Wang, Y. Li, *Sci. Rep.* **2014**, *4*, 4629–4629.
- [123] D. Usachov, O. Vilkov, A. Grüneis, D. Haberer, A. Fedorov, V. K. Adamchuk, A. B. Preobrajenski, P. Dudin, A. Barinov, M. Oehzelt, C. Laubschat, D. V. Vyalikh, *Nano Lett.* **2011**, *11*, 5401–5407.
- [124] C. Wang, K. Su, W. Wan, H. Guo, H. Zhou, J. Chen, X. Zhang, Y. Huang, *J. Mater. Chem. A* **2014**, *2*, 5018–5023.
- [125] Y. Li, Z. Li, Q. Zhang, P. K. Shen, *J. Mater. Chem. A* **2014**, *2*, 4528–4533.
- [126] C. Wang, W. Wan, J. Chen, H. Zhou, X. Zhang, L. Yuan, Y. Huang, *J. Mater. Chem. A* **2013**, *1*, 1716–1723.
- [127] G. Li, G. Li, S. Ye, X. Gao, *Adv. Energy Mater.* **2012**, *2*, 1238–1245.
- [128] Z. Wang, X. Li, Y. Cui, Y. Yang, H. Pan, Z. Wang, G. Qian, *J. Electrochem. Soc.* **2014**, *161*, A1231–A1235.
- [129] S. Lu, Y. Cheng, X. Wu, J. Liu, *Nano Lett.* **2013**, *13*, 2485–2489.
- [130] R. Chen, T. Zhao, J. Lu, F. Wu, L. Li, J. Chen, G. Tan, Y. Ye, K. Amine, *Nano Lett.* **2013**, *13*, 4642–4649.
- [131] M. Zhao, X. Liu, Q. Zhang, G. Tian, J. Huang, W. Zhu, F. Wei, *ACS Nano* **2012**, *6*, 10759–10769.
- [132] H. Peng, J. Huang, M. Zhao, Q. Zhang, X. Cheng, X. Liu, W. Qian, F. Wei, *Adv. Funct. Mater.* **2014**, *24*, 2772–2781.
- [133] C. Tang, Q. Zhang, M. Zhao, J. Huang, X. Cheng, G. Tian, H. Peng, F. Wei, *Adv. Mater.* **2014**, *26*, 6100.
- [134] X. a. Chen, Z. Xiao, X. Ning, Z. Liu, Z. Yang, C. Zou, S. Wang, X. Chen, Y. Chen, S. Huang, *Adv. Energy Mater.* **2014**, DOI: 10.1002/aenm.201301988.
- [135] K. Cai, M. Song, E. J. Cairns, Y. Zhang, *Nano Lett.* **2012**, *12*, 6474–6479.
- [136] J. Hassoun, B. Scrosati, *Angew. Chem. Int. Ed.* **2010**, *49*, 2371–2374.
- [137] W. Weng, Q. Sun, Y. Zhang, H. Lin, J. Ren, X. Lu, M. Wang, H. Peng, *Nano Lett.* **2014**, *14*, 3432–3438.
- [138] J. Hassoun, B. Scrosati, *Angew. Chem. Int. Ed.* **2010**, *49*, 2371–2374.
- [139] Y. Fu, C. Zu, A. Manthiram, *J. Am. Chem. Soc.* **2013**, *135*, 18044–18047.
- [140] M. Hagen, E. Quiroga-González, S. Dörfler, G. Fahrner, J. Tübke, M. Hoffmann, H. Althues, R. Speck, M. Krampfert, S. Kaskel, *J. Power Sources* **2014**, *248*, 1058–1066.
- [141] Y. Fu, Y. Su, A. Manthiram, *Adv. Energy Mater.* **2014**, *4*, 1–5.
- [142] Y. Fu, C. Zu, A. Manthiram, *J. Am. Chem. Soc.* **2013**, *135*, 18044–18047.
- [143] Y. Yang, G. Zheng, S. Misra, J. Nelson, M. F. Toney, Y. Cui, *J. Am. Chem. Soc.* **2012**, *134*, 15387–15394.
- [144] Y. Yang, M. T. McDowell, A. Jackson, J. J. Cha, S. S. Hong, Y. Cui, *Nano Lett.* **2010**, *10*, 1486–1491.
- [145] Y. Fu, Y. Su, A. Manthiram, *Angew. Chem. Int. Ed.* **2013**, *52*, 6930–6935.
- [146] F. Wu, J. T. Lee, A. Magasinski, H. Kim, G. Yushin, *Part. Part. Syst. Charact.* **2014**, *31*, 639–644.
- [147] J. Brückner, S. Thieme, F. Böttger-Hiller, I. Bauer, H. T. Grossmann, P. Strubel, H. Althues, S. Spange, S. Kaskel, *Adv. Funct. Mater.* **2014**, *24*, 1284–1289.
- [148] R. Elazari, G. Salitra, G. Gershinsky, A. Garsuch, A. Panchenko, D. Aurbach, *Electrochem. Commun.* **2012**, *14*, 21–24.
- [149] Y. Yan, Y. Yin, S. Xin, J. Su, Y. Guo, L. Wan, *Electrochim. Acta* **2013**, *91*, 58–61.
- [150] G. Derrien, J. Hassoun, S. Panero, B. Scrosati, *Adv. Mater.* **2007**, *19*, 2336–2340.
- [151] C. K. Chan, H. Peng, G. Liu, K. McIlwrath, X. F. Zhang, R. A. Huggins, Y. Cui, *Nat. Nanotechnol.* **2007**, *3*, 31–35.
- [152] X. Su, Q. Wu, J. Li, X. Xiao, A. Lott, W. Lu, B. W. Sheldon, J. Wu, *Adv. Energy Mater.* **2014**, *4*, 1–23.
- [153] R. Teki, M. K. Datta, R. Krishnan, T. C. Parker, T. M. Lu, P. N. Kumta, N. Koratkar, *Small* **2009**, *5*, 2236–2242.
- [154] K. Evanoff, J. Benson, M. Schauer, I. Kovalenko, D. Lashmore, W. J. Ready, G. Yushin, *ACS Nano* **2012**, *6*, 9837–9845.
- [155] S. Zheng, Y. Chen, Y. Xu, F. Yi, Y. Zhu, Y. Liu, J. Yang, C. Wang, *ACS Nano* **2013**, *7*, 10995–11003.
- [156] D. Aurbach, B. Markovsky, I. Weissman, E. Levi, Y. Ein-Eli, *Electrochim. Acta* **1999**, *45*, 67–86.
- [157] D. Aurbach, B. Markovsky, M. Levi, E. Levi, A. Schechter, M. Moshkovich, Y. Cohen, *J. Power Sources* **1999**, *81*, 95–111.
- [158] D. Aurbach, E. Zinigrad, Y. Cohen, H. Teller, *Solid State Ionics* **2002**, *148*, 405–416.
- [159] C. Huang, J. Xiao, Y. Shao, J. Zheng, W. D. Bennett, D. Lu, L. V. Saraf, M. Engelhard, L. Ji, J. Zhang, X. Li, G. L. Graff, J. Liu, *Nat. Commun.* **2014**, *4*, 3015–3021.
- [160] G. Zheng, S. W. Lee, Z. Liang, H. W. Lee, K. Yan, H. Yao, H. Wang, W. Li, S. Chu, Y. Cui, *Nat. Nanotechnol.* **2014**, *9*, 618–623.
- [161] K. Yan, H. W. Lee, T. Gao, G. Zheng, H. Yao, H. Wang, Z. Lu, Y. Zhou, Z. Liang, Z. Liu, S. Chu, Y. Cui, *Nano Lett.* **2014**, *14*, 6016–6022.
- [162] X. Cheng, H. Peng, J. Huang, F. Wei, Q. Zhang, *Small* **2014**, DOI: 10.1002/smll.201401837.
- [163] X. Zhang, W. Wang, A. Wang, Y. Huang, K. Yuan, Z. Yu, J. Qiu, Y. Yang, *J. Mater. Chem. A* **2014**, *2*, 11660–11665.
- [164] M. Koo, K. I. Park, S. H. Lee, M. Suh, D. Y. Jeon, J. W. Choi, K. Kang, K. J. Lee, *Nano Lett.* **2012**, *12*, 4810–4816.
- [165] S. Xu, Y. Zhang, J. Cho, J. Lee, X. Huang, L. Jia, J. A. Fan, Y. Su, J. Su, H. Zhang, H. Cheng, B. Lu, C. Yu, C. Chuang, T. Kim, T. Song, K. Shigeta, S. Kang, C. Dagdeviren, I. Petrov, P. V. Braun, Y. Huang, U. Paik, J. A. Rogers, *Nat. Commun.* **2013**, *4*, 1543.
- [166] Y. H. Kwon, S. W. Woo, H. R. Jung, H. K. Yu, K. Kim, B. H. Oh, S. Ahn, S. Y. Lee, S. W. Song, J. Cho, H. C. Shin, J. Y. Kim, *Adv. Mater.* **2012**, *24*, 5192–5197.
- [167] C. Zu, A. Manthiram, *Adv. Energy Mater.* **2014**, DOI: 10.1002/aenm.201400897.
- [168] Z. Yuan, H. Peng, J. Huang, X. Liu, D. Wang, X. Cheng, Q. Zhang, *Adv. Funct. Mater.* **2014**, *24*, 6105–6112.
- [169] H. Yao, G. Zheng, P. C. Hsu, D. Kong, J. J. Cha, W. Li, Z. W. Seh, M. T. McDowell, K. Yan, Z. Liang, V. K. Narasimhan, Y. Cui, *Nat. Commun.* **2014**, *5*, 3943.
- [170] J. Huang, H. Peng, X. Liu, J. Nie, X. Cheng, Q. Zhang, F. Wei, *J. Mater. Chem. A* **2014**, *2*, 10869–10875.

- [171] J. Huang, Q. Zhang, H. Peng, X. Liu, W. Qian, F. Wei, *Energy Environ. Sci.* **2014**, *7*, 347–353.
- [172] Z. Lin, Z. Liu, N. J. Dudney, C. Liang, *ACS Nano* **2013**, *7*, 2829–2833.
- [173] J. W. Park, K. Ueno, N. Tachikawa, K. Dokko, M. Watanabe, *J. Phys. Chem. C* **2013**, *117*, 20531–20541.
- [174] J. Wang, F. Lin, H. Jia, J. Yang, C. W. Monroe, Y. NuLi, *Angew. Chem. Int. Ed.* **2014**, *53*, 10099–10104.
- [175] S. Moon, Y. H. Jung, W. K. Jung, D. S. Jung, J. W. Choi, D. K. Kim, *Adv. Mater.* **2013**, *25*, 6547–6553.
- [176] X. Cheng, J. Huang, H. Peng, J. Nie, X. Liu, Q. Zhang, F. Wei, *J. Power Sources* **2014**, *253*, 263–268.

Received: August 6, 2014  
Revised: October 1, 2014  
Published online: December 15, 2014